# Precision cosmology with time delay lenses: high resolution imaging requirements

**Xiao-Lei Meng,**[1,2] **Tommaso Treu,**[2,3] **Adriano Agnello,**[2,3] **Matthew W. Auger,**[4] **Kai Liao,**[1,2,3] **Philip J. Marshall**[5]

[1]Department of Astronomy, Beijing Normal University, Beijing, 100875, China

[2]Department of Physics, University of California, Santa Barbara, CA 93106, USA

[3]Physics and Astronomy Department, University of California, Los Angeles, CA 90095-1547, USA

[4]Institute of Astronomy, University of Cambridge, Madingley Road, Cambridge CB3 0HA, UK

[5]Kavli Institute for Particle Astrophysics and Cosmology, Stanford University, 452 Lomita Mall, Stanford, CA 94305, USA

E-mail: xlmeng919@gmail.com

**Abstract.** Lens time delays are a powerful probe of cosmology, provided that the gravitational potential of the main deflector can be modeled with sufficient precision. Recent work has shown that this can be achieved by detailed modeling of the host galaxies of lensed quasars, which appear as "Einstein Rings" in high resolution images. The distortion of these arcs and counter-arcs, as measured over a large number of pixels, provides tight constraints on the difference between the gravitational potential between the quasar image positions, and thus on cosmology in combination with the measured time delay. We carry out a systematic exploration of the high resolution imaging required to exploit the thousands of lensed quasars that will be discovered by current and upcoming surveys with the next decade. Specifically, we simulate realistic lens systems as imaged by the Hubble Space Telescope (HST), James Webb Space Telescope (JWST), and ground based adaptive optics images taken with Keck or the Thirty Meter Telescope (TMT). We compare the performance of these pointed observations with that of images taken by the Euclid (VIS), Wide-Field Infrared Survey Telescope (WFIRST) and Large Synoptic Survey Telescope (LSST) surveys. We use as our metric the precision with which the slope $\gamma'$ of the total mass density profile $\rho_{tot} \propto r^{-\gamma'}$ for the main deflector can be measured. Ideally, we require that the statistical error on $\gamma'$ be less than 0.02, such that it is subdominant to other sources of random and systematic uncertainties. We find that survey data will likely have sufficient depth and resolution to meet the target only for the brighter gravitational lens systems, comparable to those discovered by the SDSS survey. For fainter systems, that will be discovered by current and future surveys, targeted follow-up will be required. However, the exposure time required with upcoming facilitites such as JWST, the Keck Next Generation Adaptive Optics System, and TMT, will only be of order a few minutes per system, thus making the follow-up of hundreds of systems a practical and efficient cosmological probe.

# Contents

## 1 Introduction

In the past few years, gravitational time delays (Refsdal 1964 [1]) have emerged as a powerful and cost effective cosmological probe. Studies based on blind analysis have shown that a single system consisting of multiple images of a background quasar (at redshift $z_s$) lensed by a foreground massive elliptical galaxy at redshift $z_d$ can be used to measure the so-called time delay distance with an uncertainty of 5-7% (Suyu et al. 2010 [2], 2013 [3], 2014 [4]). The time delay distance $D_{\Delta t}$ gives a direct measurement of the Hubble constant and allows one to break some of the main degeneracies in the interpretation of cosmic microwave background data, thus providing tight constraints on parameters such as curvature and dark energy equation of state (Coe & Moustakas 2009 [5], Linder 2011 [6], Weinberg 2013 [7], Suyu 2012 [8], Suyu et al. 2014 [4]). The time delay distance measurement of $H_0$ is comparable in terms of information content to that obtained via the cosmic distance ladder (Riess et al. 2011 [9], Freedman et al. 2012 [10]), in that is based on absolute distances and completely independent of the properties of the early universe ($z > z_s$). Importantly, time delay distances are independent of the *local* distance ladder, and thus provide a crucial test of any potential systematic uncertainties. Furthermore, being independent, the cosmic distance ladder and time delay distance constraints on $H_0$ can be statistically combined for additional gains in precision.

From an observational point of view, the attainment of precise (i.e. small random errors) and accurate (small systematic errors) time delay measurements relies on a few important ingredients. First, monitoring of the lensed quasars is required to obtain time delays with a few percent uncertainties. Dedicated monitoring campaigns have shown that this precision is achievable with 1-2m class telescopes at present time (e.g. from COMOGRAIL; Tewes et al. 2013 [11]), or in the radio

(Fassnacht et al. 2002 [12]). In the future, the exploitation of larger samples of lenses (Oguri & Marshall 2010 [13]) will require monitoring campaigns on 2-4m telescopes (Treu et al. 2013 [14]), or the deployment of long term high-cadence monitoring efforts, like the LSST (Liao et al. 2015 [15]). Second, the spectroscopic redshift of the source and deflector must be measured. For current samples, this is typically a relatively straightforward step, requiring short exposures on 4-10m class telescopes (Fassnacht & Cohen 1998 [16], Eigenbrod et al. 2007 [17]). Third, the gravitational potential of the main deflector needs to be constrained by the data so that the uncertainty on its difference between the location of the images is also of order 3%. This goal can be achieved by studying the extended structure of the lensed quasar host galaxy, and the stellar kinematics of the deflector galaxy (Treu & Koopmans 2002 [18], Koopmans et al. 2003 [19], Suyu et al. 2010 [2], Suyu et al. 2013 [3], Suyu et al. 2014 [4]). Fourth, the combined effects of the inhomogenous mass distribution along the line of sight need to be taken into account. Recent work has shown that the line of sight effects can be sufficiently characterized by measuring the properties of galaxies and weak lensing signal in the field of the main deflector, and comparing with simulated lines of sight (Suyu et al. 2010 [2], 2013 [3], 2014 [4], Greene et al. 2013 [20], Collett et al. 2013 [21]). **Fifth, the mass sheet degeneracy (Falco et al. 1985 [22]) and its generalizations (Schneider & Sluse 2013, 2014, Xu et al. 2015; [23, 24, 25]) must be broken either by the incorporation of non-lensing data such as stellar velocity dispersion (Treu & Koopmans 2002, Koopmans et al. 2003, Suyu et al. 2014, [4, 18, 19]), or by appropriate asssumptions about the mass distribution in the main deflector (Xu et al. 2015 [25]).**

However, whereas current samples have been limited to a few lenses, current and ongoing surveys—such as the Dark Energy Survey (DES), PanSTARRS1, HyperSuprimeCam (HSC)— should together discover hundreds of lensed quasars suitable for monitoring and follow-up (Oguri & Marshall 2010 [13]). During the next decade, the Large Synoptic Survey Telescope (LSST), Euclid, and the Wide-Field Infrared Survey Telescope (WFIRST) will come online, and enable the detection and measurement of an order of magnitude more, with LSST likely to provide high accuracy time delays for several hundred systems (Liao et al. 2015 [15]). These large samples will be extremely powerful cosmographic probes (Coe & Moustakas 2009 [5], Linder 2011 [6]), provided that sufficient follow-up data are available (Treu et al. 2013 [14]). In this paper we carry out a feasibility study for cosmology with future time delay lenses, focusing on the high-resolution imaging follow-up requirements. The multi-pronged nature of time delay lens follow-up makes it natural to follow the approach of addressing each component of the follow-up independently. The monitoring and spectroscopic follow-up requirements are described, for example, by Eigenbrod et al. (2005; [26]) and Linder (2015; [27]). Specifically, we aim to answer the following questions:

- Will sufficient information be available from the survey data itself, or will dedicated follow-up be necessary?

- If dedicated follow-up is necessary, approximately how much exposure time will be required per system, to enable high precision cosmography?

In order to make the problem tractable and the results general, we need a single simple metric to evaluate the quality of imaging data. In short, we need to quantify our ability to measure how the deflection angle (i.e. the derivative of the lensing potential) varies between the images, and thus how the extended images of the quasar host galaxy are stretched across the image. In practice, our ability to constrain the differential magnification will depend on the resolution of the data as well as on the number of pixels where the source is detected above a certain signal to noise ratio (and thus on the source magnification for fixed instrumental configuration and source intrinsic luminosity).

We choose to adopt as our metric the slope $\gamma'$ of the total mass density profile of the form $\rho_{tot} \propto r^{-\gamma'}$ as measured by fitting elliptical power law models to the data. This profile is the simplest one that provides a realistic description of galaxy scale lenses (Treu 2010 [28]), and the uncertainty $\gamma'$ has been shown to be approximately proportional to the uncertainty on the gravitational potential differences and thus the time delay distance, and the Hubble constant (Kochanek 2002 [29], Wucknitz 2002 [30], Suyu 2012 [8]). Intuitively, $\gamma'$ is directly related to the variations of the lensing potential. In fact, if $\gamma' = 2$ (the so-called isothermal profile) the deflection angle is constant across the image and therefore all the images will appear to have the same radial magnification. If the profile is steeper/shallower, radial magnification will vary across the image, thus giving rise to images of different widths.

Naturally, for a real measurement it is important to explore different profiles and the role of the choice of the profile in the uncertainties (see e.g. Suyu et al 2014 and references therein [4]). However, our goal is to estimate minimal requirements on the data quality. If the data quality is insufficient to constrain $\gamma'$ it will also be insufficient to constrain more flexible models. **Likewise, this paper is only concerned with precision, i.e. random errors. Systematic errors not considered in this paper, such as those arising from incomplete knowledge of the PSF will only increase the error budget (e.g., Agnello et al. 2015; Rusu et al. 2015; [31, 32]).** Thus, in order to leave room for additional sources of uncertainty in the error budget, we set a rather stringent requirement of 0.02 uncertainty of $\gamma'$ (corresponding approximately to 2% per system on time delay distance), in tests where the mock data are generated using the same model as is used in the inference of the lens parameters. In other words, our target corresponds to the requirement that the *statistical* error arising from the image quality be subdominant with respect to those arising from modeling uncertainties, time delays, and line of sight effects.

This paper is organized as follows. In Section 2, we summarize the characteristics of the telescopes and instruments simulated as part of this work. Then, in Section 3, we describe the properties of the simulated lenses. Next, in Section 4 we describe the procedure used to carry out the inference. Our results are presented in Section 5. Finally, we discuss and summarize our work in Section 6. Throughout this paper, all magnitudes are given in the AB system. Even though our findings are independent of any cosmology, we adopt a spatially flat $\Lambda$CDM cosmology with $\Omega_m = 0.3$, $\Omega_\Lambda = 0.7$, and the Hubble constant $H_0 = 70$ km s$^{-1}$ Mpc$^{-1}$ when calculating distances.

## 2 Summary of simulated instrumental setups

We aim to carry out a systematic exploration of imaging requirements given current and future facilities. For a given lens system, the instrumental setup drives our ability to constrain $\gamma'$ in a number of ways. First, the signal-to-noise ratio depends on the exposure-time adopted, sky or background noise in a chosen band, and the instrumental readout noise. Second, the pixel-size and the point-spread function (PSF) properties determine how finely one can map the system being observed, hence how robustly the deflections on either side of the lens can be quantified.

Here we summarize the main properties of instruments that will be considered in our simulations. In an effort to balance completeness with feasibility, we consider a suite of instruments that include ground and space based telescopes, and cadenced surveys where the total exposure cannot be set arbitrarily. Some of the choices are representative of a class of telescopes/instruments, for example we expect the performance of Keck Adaptive Optics to be a useful guidance for adaptive optics systems on other 8-10m class telescopes, and that of the Thirty Meter Telescope to be a guidance for other planned 20-30m class telescopes. For survey telescopes like WFIRST, LSST, and Euclid, we only consider the wide field surveys, as the deep surveys cover too small a solid angle to include randomly a useful number of lensed quasars.

Table 1 and figure 1 display the main properties of the telescopes that are needed when generating images of mock gravitational lenses, taken from the instrument websites. Figure 2 shows the typical PSF of each instrument. In order to facilitate comparisons between instruments and telescopes, whenever possible we selected the filter/band for each configuration that is closer to the $I$-band in the optical and the $K'$-band in the near infrared [1]. A brief description of each setup follows.

1. We take the Advanced Camera for Surveys (ACS) as our reference optical imager on board the Hubble Space Telescope (HST). Its properties are taken from the Space Telescope Science Institute HST Exposure Time Calculator.[2] In the chosen F814W filter its performance is comparable to that of WFC3 (slightly higher sensitivity and coarser pixel size). For simplicity, we neglect charge transfer inefficiency effects, assuming that they are negligible or can be corrected to the desired level. The PSF is simulated using the Tiny Tim software (Krist 1993 [35]).

2. The Near Infrared Camera (NIRCAM) on board the James Webb Space Telescope (JWST) is chosen as the next space based imaging capability. We select the broad F200W filter, where the image quality is virtually diffraction limited. We use the instrument properties as given by the JWST Exposure Time Calculator.[3]

3. The current and planned adaptive optics systems (hereafter LGSAO & NGAO;[36], [37], respectively) at the W.M.Keck Observatory are chosen to represent current and upcoming AO performance on 8-10m class telescopes. We consider the current instrument NIRC2, although further gains might be possible with an instrument upgrade in conjuction with the AO system upgrade. We also assume conservatively the same background for NGAO as with LGSAO, even though the thermal background should be significantly lower for NGAO, due to the lower operating temperature of the NGAO system. We adopt the typical configuration used for studies of gravitational lens systems (Fassnacht & Cohen 1998 [16]): $K'$ filter, MCDS readout mode, read number $N = 16$, and narrow camera mode. A real observed PSF is used for the current AO system. The simulated PSF and performance characteristics of NGAO have been kindly provided by the NGAO team.

4. The infrared imager and spectrograph IRIS (Larkin et al. 2010 [38]) working behind adaptive optics on the Thirty Meter Telescope (TMT) is selected to represent the performance of the extremely large telescopes that will be operational in the next decade. IRIS is expected to be close to diffraction limited in the $K'$ band. The simulated PSF and performance characteristics of TMT-IRIS have been obtained from the IRIS team, from the TMT Exposure Time Calculator (ETC) [4] and from the paper by Do et al. (2014) [39].

5. Euclid is a space survey telescope planned to be launched by the European Space Agency. Euclid has two instruments: a high-resolution visible imager, and a NIR imaging spectrograph. We study the performance of the high-resolution visible imager, the more suitable to detailed gravitational lensing work, with the standard survey parameters. The instrument properties are taken from Schweitzer et al. 2010 [40], Penny et al. 2013 [41] and Cropper et al. 2014 [42].

---

[1]Clearly, for survey telescopes such as LSST one can further increase the precision on $\gamma'$ by considering multiple bands at once, when they are available (Newton et al. 2011 [33], Auger et al. 2013 [34]). However, the multifilter analysis is beyond the scope of this paper, which is concerned with comparison across instruments/telescopes.

[2]http://etc.stsci.edu

[3]http://jwstetc.stsci.edu

[4]http://tmt.mtk.nao.ac.jp/ETC_readme.html

Since the PSF is proprietary to the Euclid team, we adopt for simplicity a Gaussian function with full width half maximum $0.''18$.

6. We study the survey mode of the 2.4m WFIRST space mission, focusing on the 2000 square degree HLS Imaging Survey in the F184W filter. The instrument/survey properties are based on the WFIRST-Astrophysics Focused Telescope Assets Final Report (by the Science Definition Team and WFIRST Project, Spergel et al. 2013 [43]) and the WFIRST ETC. [5] Since the final PSF was not available at the time of this writing we adopt a Gaussian function with FWHM $0.''15$. As an additional test, in order to investigate the sensitivity of our estimates to the choice of the PSF, we repeat the simulations assuming a Moffat (1969; [?] ) PSF, with different shape parameters.

7. The Large Synoptic Survey Telescope (LSST) is designed to repeatedly image the entire visible Southern sky in six optical and near infrared bands (out to $\sim 1$ micron) every few nights for ten years. We take the survey and instrument properties from Ivezic et al. 2008 [44] and the LSST Science Requirements Document.[6] The PSF of LSST will vary over time. We adopt a Gaussian PSF with FWHM $0.''7$ as representative of the stacked image quality of LSST in the i-band, and consider the full depth survey images in our analysis.

We do not consider radio interferometers like ALMA or VLBI, given the radically different properties of the data, and the need for additional assumptions relating the optical/IR light to the radio emission. An assessment of their ability to provide sufficiently accurate high resolution images for cosmography is left for future work.

## 3 The Lens Sample

In this section we introduce our sample, taken to be illustrative of the kind of systems to be discovered in the next decade.

### 3.1 Sample Selection

We have chosen four prototypical systems for this exploration, characterized as *faint* or *bright* and *double* or *quad* depending on the photometry and image configuration. This set of four main choices covers regimes with different numbers of pixels above a certain S/N, which in turn depend on the number of images produced by the lens.

The brighter lenses are selected to be representative of the majority of currently known lenses, selected from the Sloan Digital Sky Survey, while the fainter lenses are selected to be representative of the fainter systems to be discovered in current and future surveys within the next decade (Oguri & Marshall 2010 [13]). We expect that the systems to be used to measure time delay distances in the next decade will span approximately the range covered by our sample. Note that some known lensed quasars are significantly brighter than any of the systems simulated here (e.g., Patnaik et al. 1992 [45]). Even though we expect more of those to be discovered in the near future and they will be useful, they will not represent the majority of the systems in future large samples, nor present any major challenge for follow-up, so we do not consider them here.

To remain as realistic as possible, the brighter mocks are based upon lenses in the Sloan Lens ACS Survey (SLACS; Bolton et al. 2006 [46], Treu et al. 2006 [47], Koopmans et al. 2006 [48],

---

[5]http://wfirst-web.ipac.caltech.edu/wfDepc/wfDepc.jsp?etc
[6]http://www.lsst.org/files/docs/SRD.pdf

Gavazzi et al. 2007 [49], Bolton et al. 2008a [50], Gavazzi et al. 2008 [51], Bolton et al. 2008b [52], Treu et al. 2009 [53], Auger et al. 2009 [54], Auger et al. 2010 [55], Newton et al. 2011 [33], Shu et al. 2015 [56], Papers I-XII, respectively) and the fainter mocks on the Strong Lensing Legacy Survey (SL2S; More et al. 2012 [57], Gavazzi et al. 2012 [58], Ruff et al. 2011 [59], Sonnenfeld et al. 2013 [60], Sonnenfeld et al. 2013 [61], Sonnenfeld et al. 2015 [62], Papers I-V, respectively, except for the first citation) samples.

**The sources are set at $z_s$ = 1.071 and 2.77 and the deflectors are set at $z_d$ = 0.351 and 0.783, respectively for the bright and faint systems. The redshifts are taken from the real systems used as an inspiration for this study, and are well within the range of the redshifts that we expect to find in future samples of lensed quasars (e.g. Oguri & Marshall 2010; [13]). A different choice within a realistic range would not have changed any of our conclusions.**

## 3.2 Parameters of the Sample of Mock Lenses

The structural parameters of the four systems are listed in Table 2 and Table 3. When not explicitly known from existing data, mock model parameters are assigned via plausibility arguments as specified below. The source and deflector of the *bright* lens system configurations are built along SLACS J0330-0020 as modelled by Bolton et al. 2008a (SLACS V, [50]), Auger et al. 2009 (SLACS IX, [54]), and Newton et al. 2011 (SLACS XI, [33]). For the *faint* lens system configuration, the source and deflector have parameters from the Sonnenfeld et al. 2013 (SL2S III, [60]) model of SL2S J135949+553550 (also, Sonnenfeld, A., 2015, private communication).

Source and deflector magnitudes in the *bright* case for $I$ and $V$ bands are from Newton et al. 2011 [33], for $K$-band are estimated based on the other colors, and typical spectral energy distributions, i.e. an early-type galaxy for the deflector and a star forming galaxy for the source. Meanwhile, source magnitudes in the *faint* case are arbitrarily set to 25.0 in all bands. Deflector magnitudes in the *faint* case are not directly available from the data, so they require some extrapolations. The value for $I$-band is based on Sonnenfeld et al. 2013 (SL2S III, [60]), while for $K$ and $V$ bands are estimated with K-corrections from typical spectral energy distributions. Unknown magnitudes in $K$-band are assigned from $H$-band ones via $K_{AB} = H_{AB}$. We note that the host galaxies of type-1 AGNs at these redshifts are generally brighter than the magnitudes adopted here (Bennert et al. 2011; [63]), so our assumptions are quite conservative.

The effective (half-light) radii to be fitted in *bright* systems are evaluated separately in different bands, to get a precise estimate of the effective radius and its uncertainties. Differently, a unique effective radius is asserted across bandpasses for the *faint* systems. Neglecting color gradients in this case does not affect the ability to recover the mass density profile in any significant way (Sonnenfeld et al. 2013 [60]).

For both the *faint* and the *bright* systems, the source positions are assigned so as to map the source in either two or four images. This choice allows us to explore whether the number of images makes any substantial difference while keeping the other properties of the systems fixed.

In order to construct realistic systems for time delay measurements, point sources must be added to represent the lensed quasars. As described in the next section this is done in the image plane, in order to gain computational precision and efficiency. The magnification at the location of the quasar images is calculated by solving the lens equation using `gravlens` [64]. The source-plane magnitudes of the point sources are chosen to be somewhat brighter then the host galaxy, as it is typically the case for medium luminosity AGN (e.g., Bennert et al. 2011 [65]), and have realistic colors for AGN at the source redshits. The adopted magnitudes are listed in Table 4.

We note that the *bright* source configuration is too bright to be practical for TMT, given its sensitivity – the exposure time scales as $D^{-4}$, where $D$ is the telescope diameter, for background lim-

ited point source exposures. Realistically, observations of such bright systems would be completely dominated by overheads related to target acquisition and will only be carried out in extremely rare circumstances. Therefore we do not simulate TMT observations for the bright systems. Even for the fainter system, we have chosen to make the AGN artificially fainter ($K$=26.0) in order to avoid saturating the central pixels while imaging deep enough to get a sufficient signal to noise ratio on the host galaxy. As will be shown below, the exposure time requirements for TMT are short even in these cases.

## 4 Description of the inference process

In this section, we summarize the process of modeling the mock lens systems. By comparing the distribution of the ratio between the inferred values and the input, we obtain the desired estimate of the statistical precision with which each parameter can be determined. As motivated in the introduction, we are interested primarily in the mass density profile slope $\gamma'$. Therefore, we will only show the statistics for that parameter, even though all the parameters are varied simultaneously during the inference. We first describe the image generating process in Section 4.1, and then we describe the inference process in Section 4.2.

### 4.1 Image generating process

Before we fit the mock lens system we need to define the models to describe the source galaxy light, the lens galaxy light, and the lens mass. We start with the surface brightness distribution of the source and lens galaxies. The correspondence between image-plane and source-plane is given via the deflection angles, which in turn depend on the mass distribution of the lens. A PSF is used to convolve the light of lens galaxy, lensed source galaxy and point-source. Finally, we introduce counts noise, readout noise, and background noise. These steps are described in this subsection.

#### 4.1.1 Light Model

We use the Sérsic profile (Sérsic 1963 [66], 1968 [67]) to describe the surface brightness profiles of the sources and the deflectors. The Sérsic profile is described by

$$I(R) = I_{\mathrm{e}} \exp\left[-k\left(\left(\frac{R}{R_{\mathrm{eff}}}\right)^{\frac{1}{n}} - 1\right)\right], \tag{4.1}$$

$$R(x, y, q) = \sqrt{qx^2 + y^2/q}. \tag{4.2}$$

The amplitude $I_{\mathrm{e}}$ is the intensity at the effective radius $R_{\mathrm{eff}}$, the Sérsic index $n$ controls the degree of curvature of the radial light profile, the constant $k$ is determined so that $R_{\mathrm{eff}}$ is the half light radius (Ciotti & Bertin 1999 [68]), and $q$ denotes the axis ratio. Empirically, $n$ increases with galaxy luminosity, most galaxies being fitted by Sérsic index in the range $0.6 \leq n \leq 10.0$ (Merritt et al. 2006 [69]). We adopt $n = 4$ for the deflectors, typical of massive early-type galaxies, and $n = 4/3$ or $n = 4$ for the sources, consistent with typical observed values for blue galaxies and AGN hosts. We checked by re-running simulations with different $n$ for the source that our results do not depend significantly on this model assumption.

#### 4.1.2 Mass Model

The lens mass profile is assigned within a class of power-law models,

$$\Sigma(x, y) = \Sigma_{cr} \frac{3 - \gamma'}{1 + q_{\mathrm{m}}} \left(\frac{\sqrt{X^2 + q_{\mathrm{m}}^{-2}Y^2}}{R_{\mathrm{E}}}\right)^{1-\gamma'}, \tag{4.3}$$

where $q_{\mathrm{m}}$ is the axis ratio, $\gamma'$ is the radial power-law slope, the $\{X, Y\}$ principal axes are rotated by the lens position angle w.r.to the canonical $x$ (increasing to the West) and $y$ (increasing to the North). Within this functional family, the deflections scale as $R^{2-\gamma'}$ with distance from the lens. The *critical density* $\Sigma_{cr}$ is defined by

$$\Sigma_{\mathrm{cr}} = \frac{c^2 D_{\mathrm{s}}}{4\pi G D_{\mathrm{d}} D_{\mathrm{ds}}} \tag{4.4}$$

in terms of the relative distances to the deflector ($D_{\mathrm{d}}$), to the source ($D_{\mathrm{s}}$), and between the deflector and the source ($D_{\mathrm{ds}}$). The Einstein radius $R_{\mathrm{E}}$ is chosen such that, in the spherical limit ($q_{\mathrm{m}} = 1$), it encloses a mean surface density equal to $\Sigma_{cr}$. This is also the radius of a ring traced by the host of the quasar when this is exactly aligned with the lens galaxy.

Power-law models of elliptical galaxies (Evans 1994 [70]) have often been used with success over the years to model gravitational lenses. Fast methods to compute 2D deflections from elliptical power-law profiles have been given by Barkana 1998 [71], as a special case of the formalism by Schramm 1990 [72] for homoeoidal profiles.

Lensed image profiles are obtained by inverse ray shooting. First, each pixel position in the image plane is mapped back to the source plane via its corresponding deflection angle. Then, we exploit the fact that surface brightness is preserved by lensing to assign surface brightnesses from our putative source models to each detector pixel in the image plane. Finally, we convolve these images with the PSF appropriate for each instrument, yielding mock observations of the AGN host galaxy Einstein rings.

### 4.1.3 Point Source Model

In order to reduce computation time and complexity, the point source images are added to the light model by adding a PSF with appropriate normalization and position directly to the image plane. The normalization and position of the images for the center of the source in the source plane are computed for each configuration by solving the lens equation using `gravlens` [64].

### 4.1.4 Image Noise

In the final step of our simulations we account for the effect of noise arising from the counts statistics, the background, and detector read out. As usual, the variance of noise per pixel is given by

$$\mathrm{Var}_{\mathrm{pix}} = \sqrt{Ct + B \cdot t + N_{\mathrm{read}} R^2} \tag{4.5}$$

where $C$ is the signal from clean lens system in electrons per second per pixel, $t$ is the integration time in seconds, $B$ is the sum of the sky background and detector dark current in electrons per second per pixel, $N_{\mathrm{read}}$ is the number of detector readouts, and $R$ is the standard deviation of the read noise in electrons. Realistically, when long integration times are required, we set the number of readouts by requiring no single exposure be longer then a maximum time that depends on each instrument configuration. Considering the definite properties in different types of instruments, we pick 1000.0 seconds as the crude maximum exposure time for space telescopes (HST and JWST), 300.0 seconds for the ground based telescopes (Keck and TMT) appropriately. Each of the surveys we model (Euclid, WFIRST, and LSST) have fixed maximum exposure times (590 seconds, 184 seconds, and 15 seconds, respectively) which we use to compute the read noise per exposure. We then emulate the stacking of each survey's exposures to reach the approximate expected total exposure time (2360, 920 and 4500 seconds, for Euclid, WFIRST, and LSST, respectively). Examples of simulated images are shown in Figure 3 to 6.

## 4.2 Inferring the parameters

The same code that is used to generate the mock Einstein Ring images is also used to fit them. The modelling procedure follows previous work done with real lens data (e.g., Auger et al. 2011 [73], Auger et al. 2013 [34], Stark et al. 2013 [74]). We fit for the following non-linear parameters: position, half light radius, axis ratio of light, position angle, and Sérsic index for the source and deflector brightness model (12 parameters); position, Einstein radius, the axis ratio of the mass distribution, position angle, and power-law slope for the deflector mass model (6 parameters); and QSO positions in the image plane (4 parameters for two-image lenses, 8 parameters for four-image systems). We note in particular that due to e.g., microlensing, millilensing, and differential reddening, the positions and fluxes of the QSO images are not tied to the lens model and they are therefore in effect treated as 'foreground' stars. Most priors on the non-linear parameters are taken to be uniform, but the prior on the position of the deflector mass is tied to the position of the deflector surface brightness; the mass is generally close to coincident with the light in galaxy-scale lenses. The fluxes/amplitudes of each of the surface brightness components (the source and deflector galaxies and the QSO images) are linear parameters and are determined by linear inversion for any given set of proposed non-linear paramerters.

The goodness of fit is assessed through the standard image-plane $\chi^2$, by comparing the model and mock data surface brightness profiles. Uncertainties are obtained via MCMC exploration of the posterior, with the fluxes implicitly marginalized over. The likelihood is simply given by $\mathcal{L} \propto \exp[-\chi^2/2]$.

The mock data images for different instruments are all $4'' \times 4''$, corresponding to the pixel numbers of $80 \times 80$ for HST, $130 \times 130$ for JWST, $400 \times 400$ for Keck (both LGSAO and NGAO), $1000 \times 1000$ for TMT, $40 \times 40$ for Euclid, $36 \times 36$ for WFIRST, $20 \times 20$ for LSST approximately. The sampling numbers are fixed at 60000 for each inference progress. The acceptance ratios remain stable between 20% ~ 30%. Based on the parameters above mentioned, the inference is computationally expensive: typical run times range between 15 minutes and 4000 minutes per system on a linux desktop computer. In more specific terms, ~ 100 minutes for HST, ~ 150 minutes for JWST, ~ 300 minutes for Keck (both LGSAO and NGAO), ~ 4000 minutes for TMT, ~ 40 minutes for Euclid and WFIRST, ~ 15 minutes for LSST.

## 4.3 Exposure times

The goal of this work is to investigate what combinations of instrument/telescope configuration and exposure time produce images of quality sufficient to determine $\gamma'$ with 0.02 precision.

For the telescopes/instruments operated in observatory mode, we are able to set the exposure time to any desired level. The minimum exposure time required is defined as the "target" exposure time. In addition, in order to quantify how the precision on $\gamma'$ depends on exposure time, we also simulated images with 1/3 and 3× the target exposure time. This is meant to provide useful guidance for designing future experiments. However, for some combination of lens brightness and telescope/instrument configuration, the target exposure time is too short to be adopted in realistic observations. In practice, therefore these lenses will either not be observed with this setup or be observed for longer exposure time. Taking into account typical overheads for pointing and acquisition we evaluated that the brighter lenses are too bright to be observed with TMT. Likewise the brighter systems are likely too bright to be observed efficiently with JWST. We still simulated them, but set the minimum exposure time to 60s. Of course in some instances it may be beneficial to obtain longer exposures with JWST and TMT and thus exquisite data.

For the survey telescopes, we simulated the planned exposure time as described above, and then simply considered the specific question of whether the ensuing data quality is sufficient to meet the requirement or not.

## 5  Results

Using the methods summarized in the previous section we generate 30 mock systems for most configurations and 10 mock systems for TMT with the view of saving computing time, and carry out the full inference for each one using the python Markov Chain Monte Carlo sampler pymc. The results are summarized in Figures 7 to 10. Table 5 summarizes the "target" exposure times for HST, JWST, Keck LGSAO and NGAO, TMT, i.e. those required in order to reach 0.02 uncertainties on $\gamma'$. We reiterate that this is is only the random component of the uncertainty, and thus it represents a lower limit to the total uncertainty. For this reason we have set a rather stringent limit of 0.02, in order to leave room for additional uncertainties, such as, e.g., systematic errors related to PSF reconstruction and modeling errors. In practice, our target exposure times should be considered as minimum exposure times, i.e. necessary and not sufficient conditions. Assessing the contribution of those additional sources of uncertainty requires detailed modeling of specific systems and instruments (e.g., Suyu et al. 2014 [4]), and is left for future work.

First of all, we find that HST can deliver the desired image quality with exposures of a few kiloseconds at most, consistent with published work (Suyu et al. 2013 [3]). Conversely, it seems that current AO capabilities – even setting aside the difficulties associated with the reconstruction of the PSF – are only sufficient to study the brighter systems, for reasonable exposure times. The improvement with NGAO will be substantial, cutting integration times down to HST-like for both the bright and the faint lenses. In this case, the higher background than from space is compensated by the advantage of having smaller detector pixels, and thus better sampling of the PSF, and a larger telescope aperture. The NGAO performance may further improve if the thermal background is reduced with respect to LGSAO as planned and if the instrument has higher throughput than NIRC2.

For TMT we concluded that 1200s of exposure will be more than sufficient for all systems considered here and therefore TMT is likely to be used either in "snapshot mode" or to take an image before taking a spectrum for determining the deflector velocity field and source redshift, or to follow-up fainter systems, yet to be discovered. Similarly, JWST can obtain images of the desired quality in just a few minutes, and therefore it is likely to be used mostly to take images before taking a spectrum or to follow-up fainter systems.

For the surveys, the conclusion is that while the Euclid survey seems to have insufficient depth and resolution to meet our requirements on the targets considered here, LSST and WFIRST should be sufficient at least for the brighter ones. Of course, these surveys will cover vast fractions of the sky and will therefore provide useful images for all the brighter systems (Koopmans et al. 2009 [75]) at no additional cost. Those will be a great complement to the deeper pointed observation obtained with the other telescopes. WFIRST is planned to have a component of GO program, so it could meet the imaging requirements by integrating longer than in the survey mode. In fact, WFIRST is expected to have imaging performance superior to that of WFC3 on board HST, which has already been used to perform studies of time delay lenses, using integration times of a few orbits per system (~10ks; HST-GO-12889, PI: Suyu). **Amongst the surveys considered here and modeled with a Gaussian PSF, WFIRST is the one with most potential for this application. Therefore, it is worth checking that our conclusion does not depend on the assumption of a Gaussian PSF. In order to verify this we**

have repeated our simulations adopting a more generic Moffat profile ([? ])

$$\frac{\beta - 1}{\pi \alpha^2} \left[ 1 + \left( \frac{r}{\alpha} \right)^2 \right]^{-\beta} \tag{5.1}$$

for the PSF, keeping the FWHM=$2\alpha \sqrt{2^{1/\beta} - 1}$ fixed and varying the shape parameter $\beta$. The results of the simulations are summarized in Table 6. The precision on $\gamma'$ decreases only slightly as the wings of PSF become more important (i.e. smaller $\beta$), showing that our conclusions are robust to the choice of the PSF shape, as long as that is known.

# 6 Summary

Gravitational time delays are a powerful tool for cosmography. Transforming measured time delays into time distances requires modeling the gravitational potential of the main deflector with sufficient accuracy. Recent work has shown that this is possible provided that images of sufficient resolution and signal to noise ratio are available. In anticipation of the hundreds to thousands of lensed quasars that are going to be discovered in the next decade from ground based low resolution imaging surveys (Oguri & Marshall 2010 [13]), we study the requirements for high resolution imaging follow-up. We consider a range of instrument/telescope configurations spanning from currently available systems (HST/ACS and Keck/LGSAO/NIRC2) to planned observatories and surveys from space (JWST/NIRCAM, Euclid, WFIRST/HLS) and from the ground (Keck/NGAO/NIRC2, TMT/IRIS). In order to carry out a generic and systematic comparison across multiple telescopes we simulate four realistic lens systems, spanning the range of magnitudes and configuration expected for lenses to be discovered in the next decade. We also define a single metric, which is the ability to measure the slope of the mass density profile of an elliptical power law mass density profile. In order to guarantee that the images be sufficient to constrain the Fermat potential to a level so that the random uncertainties are subdominant with respect to other sources of uncertainty, we consider it necessary for them to contain enough information to constrain $\gamma'$ with 0.02 precision or better, which corresponds approximately to a 2% precision on time delay distance and hence $H_0$. We find that:

- Our simulations show that HST can provide sufficient information with integration times of order 1-10ks, consistent with recent work based on real data.

- Keck/LGSAO can provide sufficient information for the brighter systems to be discovered. The critical issue will be the accuracy with which the PSF can be reconstructed. Significant effort is under way to overcome this obstacle (Jolissaint et al. 2014 [76], Ragland et al. 2014 [? ]).

- The planned Keck/NGAO system will improve the performance of Keck to make it comparable to that of HST, again provided that the PSF can be reconstructed with sufficient accuracy.

- JWST/NIRCAM and TMT/IRIS will be able to deliver the desired image quality with short exposure times for any lens for which time delays are reasonably going to be available. Thus they will be ideal instruments for follow-up of time-delay lenses, especially if short images are followed by deeper spectroscopic observations to measure the redshift of the source and the spatially resolved velocity dispersion (and redshift) of the deflector. For TMT, and other ELTs, the abilty to reconstruct accurately the PSF of the AO system (Herriot et al. [77]) will be critical for time delay cosmography.

- The survey modes of Euclid/WFIRST/LSST will likely be too shallow and/or have insufficient resolution except for the very brightest systems in the sky. Thus Euclid/WFIRST/LSST will make major contributions in the area of discoveries of these systems, but follow-up will be necessary for the fainter ones, for example with WFIRST in general observer mode.

We conclude by emphasizing that our study is only concerned with precision, i.e. the study of random uncertainties. For this reason we have chosen a target precision of 0.02 on $\gamma'$, that would be a subdominant contribution to the total error budget for the best currently studied systems. This is intended to leave room for additional sources of systematic uncertainty. Within instrumental effects, an important term will stem from uncertainties in the knowledge of the PSF. Studies based on the comparison of multiple Hubble Space Telescope optical images have shown that in this case residual PSF uncertainties do not contribute more than the estimated total uncertainties. However, the contribution of the PSF to the total error budget may be more important for ground based Adaptive Optics data and future telescopes. Significant work is under way to characterize this source of uncertainty based on existing data (Rusu et al. 2015; [32]; Suyu et al. 2015, in preparation), even though we are not aware of a systematic investigation of the PSF-related uncertainties on the time-delay distance. We plan to carry out such a systematic investigation in the near future.

## References

[1] S. Refsdal, *On the possibility of determining Hubble's parameter and the masses of galaxies from the gravitational lens effect*, Mon. Not. R. Astron. Soc. **128** (1964) 307.

[2] S. H. Suyu, P. J. Marshall, M. W. Auger, S. Hilbert, R. D. Blandford, L. V. E. Koopmans, C. D. Fassnacht, and T. Treu, *Dissecting the Gravitational lens B1608+656. II. Precision Measurements of the Hubble Constant, Spatial Curvature, and the Dark Energy Equation of State*, Astrophys. J. **711** (Mar., 2010) 201–221, [`arXiv:0910.2773`].

[3] S. H. Suyu, M. W. Auger, S. Hilbert, P. J. Marshall, M. Tewes, T. Treu, C. D. Fassnacht, L. V. E. Koopmans, D. Sluse, R. D. Blandford, F. Courbin, and G. Meylan, *Two Accurate Time-delay Distances from Strong Lensing: Implications for Cosmology*, Astrophys. J. **766** (Apr., 2013) 70, [`arXiv:1208.6010`].

[4] S. H. Suyu, T. Treu, S. Hilbert, A. Sonnenfeld, M. W. Auger, R. D. Blandford, T. Collett, F. Courbin, C. D. Fassnacht, L. V. E. Koopmans, P. J. Marshall, G. Meylan, C. Spiniello, and M. Tewes, *Cosmology from Gravitational Lens Time Delays and Planck Data*, Astrophys. J. **788** (June, 2014) L35, [`arXiv:1306.4732`].

[5] D. Coe and L. A. Moustakas, *Cosmological Constraints from Gravitational Lens Time Delays*, Astrophys. J. **706** (Nov., 2009) 45–59, [`arXiv:0906.4108`].

[6] E. V. Linder, *Lensing time delays and cosmological complementarity*, Phys. Rev. D **84** (Dec., 2011) 123529, [arXiv:1109.2592].

[7] D. H. Weinberg, M. J. Mortonson, D. J. Eisenstein, C. Hirata, A. G. Riess, and E. Rozo, *Observational probes of cosmic acceleration*, Phys. Rept. **530** (Sept., 2013) 87–255, [arXiv:1201.2434].

[8] S. H. Suyu, *Cosmography from two-image lens systems: overcoming the lens profile slope degeneracy*, Mon. Not. R. Astron. Soc. **426** (Oct., 2012) 868–879, [arXiv:1202.0287].

[9] A. G. Riess, L. Macri, S. Casertano, H. Lampeitl, H. C. Ferguson, A. V. Filippenko, S. W. Jha, W. Li, and R. Chornock, *A 3% Solution: Determination of the Hubble Constant with the Hubble Space Telescope and Wide Field Camera 3*, Astrophys. J. **730** (Apr., 2011) 119, [arXiv:1103.2976].

[10] W. L. Freedman, B. F. Madore, V. Scowcroft, C. Burns, A. Monson, S. E. Persson, M. Seibert, and J. Rigby, *Carnegie Hubble Program: A Mid-infrared Calibration of the Hubble Constant*, Astrophys. J. **758** (Oct., 2012) 24, [arXiv:1208.3281].

[11] M. Tewes, F. Courbin, G. Meylan, C. S. Kochanek, E. Eulaers, N. Cantale, A. M. Mosquera, P. Magain, H. Van Winckel, D. Sluse, G. Cataldi, D. Vörös, and S. Dye, *COSMOGRAIL: the COSmological MOnitoring of GRAvItational Lenses. XIII. Time delays and 9-yr optical monitoring of the lensed quasar RX J1131-1231*, A&A **556** (Aug., 2013) A22, [arXiv:1208.6009].

[12] C. D. Fassnacht, E. Xanthopoulos, L. V. E. Koopmans, and D. Rusin, *A Determination of $H_0$ with the CLASS Gravitational Lens B1608+656. III. A Significant Improvement in the Precision of the Time Delay Measurements*, Astrophys. J. **581** (Dec., 2002) 823–835, [astro-ph/0208420].

[13] M. Oguri and P. J. Marshall, *Gravitationally lensed quasars and supernovae in future wide-field optical imaging surveys*, Mon. Not. R. Astron. Soc. **405** (July, 2010) 2579–2593, [arXiv:1001.2037].

[14] T. Treu, P. J. Marshall, F.-Y. Cyr-Racine, C. D. Fassnacht, C. R. Keeton, E. V. Linder, L. A. Moustakas, M. Bradac, E. Buckley-Geer, T. Collett, F. Courbin, G. Dobler, D. A. Finley, J. Hjorth, C. S. Kochanek, E. Komatsu, L. V. E. Koopmans, G. Meylan, P. Natarajan, M. Oguri, S. H. Suyu, M. Tewes, K. C. Wong, A. I. Zabludoff, D. Zaritsky, T. Anguita, R. J. Brunner, R. Cabanac, E. E. Falco, A. Fritz, G. Seidel, D. A. Howell, C. Giocoli, N. Jackson, S. Lopez, R. B. Metcalf, V. Motta, and T. Verdugo, *Dark energy with gravitational lens time delays*, ArXiv e-prints (June, 2013) [arXiv:1306.1272].

[15] K. Liao, T. Treu, P. Marshall, C. D. Fassnacht, N. Rumbaugh, G. Dobler, A. Aghamousa, V. Bonvin, F. Courbin, A. Hojjati, N. Jackson, V. Kashyap, S. Rathna Kumar, E. Linder, K. Mandel, X.-L. Meng, G. Meylan, L. A. Moustakas, T. P. Prabhu, A. Romero-Wolf, A. Shafieloo, A. Siemiginowska, C. S. Stalin, H. Tak, M. Tewes, and D. van Dyk, *Strong Lens Time Delay Challenge. II. Results of TDC1*, Astrophys. J. **800** (Feb., 2015) 11, [arXiv:1409.1254].

[16] C. D. Fassnacht and J. G. Cohen, *Keck spectroscopy of three gravitational lens systems discovered in the JVAS and CLASS surveys*, Astron. J. **115** (Feb., 1998) 377, [astro-ph/9711044].

[17] A. Eigenbrod, F. Courbin, and G. Meylan, *COSMOGRAIL: the COSmological MOnitoring of GRAvItational Lenses. VI. Redshift of the lensing galaxy in seven gravitationally lensed quasars*, A&A **465** (Apr., 2007) 51–56, [astro-ph/0612419].

[18] T. Treu and L. V. E. Koopmans, *The internal structure of the lens PG1115+080: breaking degeneracies in the value of the Hubble constant*, Mon. Not. R. Astron. Soc. **337** (Dec., 2002) L6–L10, [astro-ph/0210002].

[19] L. V. E. Koopmans, T. Treu, C. D. Fassnacht, R. D. Blandford, and G. Surpi, *The Hubble Constant from the Gravitational Lens B1608+656*, Astrophys. J. **599** (Dec., 2003) 70–85, [astro-ph/0306216].

[20] Z. S. Greene, S. H. Suyu, T. Treu, S. Hilbert, M. W. Auger, T. E. Collett, P. J. Marshall, C. D. Fassnacht, R. D. Blandford, M. Bradač, and L. V. E. Koopmans, *Improving the Precision of Time-delay Cosmography with Observations of Galaxies along the Line of Sight*, Astrophys. J. **768** (May, 2013) 39, [arXiv:1303.3588].

[21] T. E. Collett, P. J. Marshall, M. W. Auger, S. Hilbert, S. H. Suyu, Z. Greene, T. Treu, C. D. Fassnacht, L. V. E. Koopmans, M. Bradač, and R. D. Blandford, *Reconstructing the lensing mass in the Universe from photometric catalogue data*, Mon. Not. R. Astron. Soc. **432** (June, 2013) 679–692, [arXiv:1303.6564].

[22] E. E. Falco, M. V. Gorenstein, and I. I. Shapiro, *On model-dependent bounds on H(0) from gravitational images Application of Q0957 + 561A,B*, Astrophys. J. **289** (Feb., 1985) L1–L4.

[23] P. Schneider and D. Sluse, *Mass-sheet degeneracy, power-law models and external convergence: Impact on the determination of the Hubble constant from gravitational lensing*, A&A **559** (Nov., 2013) A37, [arXiv:1306.0901].

[24] P. Schneider and D. Sluse, *Source-position transformation: an approximate invariance in strong gravitational lensing*, A&A **564** (Apr., 2014) A103, [arXiv:1306.4675].

[25] D. Xu, D. Sluse, P. Schneider, V. Springel, M. Vogelsberger, D. Nelson, and L. Hernquist, *Lens galaxies in the Illustris simulation: power-law models and the bias of the Hubble constant from time-delays*, *ArXiv e-prints* (July, 2015) [arXiv:1507.0793].

[26] A. Eigenbrod, F. Courbin, C. Vuissoz, G. Meylan, P. Saha, and S. Dye, *COSMOGRAIL: The COSmological MOnitoring of GRAvItational Lenses. I. How to sample the light curves of gravitationally lensed quasars to measure accurate time delays*, A&A **436** (June, 2005) 25–35, [astro-ph/0503019].

[27] E. V. Linder, *Tailoring strong lensing cosmographic observations*, Phys. Rev. D **91** (Apr., 2015) 083511, [arXiv:1502.0135].

[28] T. Treu, *Strong Lensing by Galaxies*, Annu. Rev. Astron. Astrophys. **48** (Sept., 2010) 87–125, [arXiv:1003.5567].

[29] C. S. Kochanek, *What Do Gravitational Lens Time Delays Measure?*, Astrophys. J. **578** (Oct., 2002) 25–32, [astro-ph/0205319].

[30] O. Wucknitz, *Degeneracies and scaling relations in general power-law models for gravitational lenses*, Mon. Not. R. Astron. Soc. **332** (June, 2002) 951–961, [astro-ph/0202376].

[31] A. Agnello, A. Sonnenfeld, S. H. Suyu, T. Treu, C. D. Fassnacht, C. Mason, M. Bradač, and M. W. Auger, *High resolution imaging and spectroscopy of the gravitational lens SDSSJ1206+4332: a natural coronagraph at $z=1.789$ and a standard ruler at $z=0.745$*, MNRAS, submitted, ArXiv:1506.02720 (June, 2015) [arXiv:1506.0272].

[32] C. E. Rusu, M. Oguri, Y. Minowa, M. Iye, N. Inada, S. Oya, I. Kayo, Y. Hayano, M. Hattori, Y. Saito, M. Ito, T.-S. Pyo, H. Terada, H. Takami, and M. Watanabe, *Subaru Telescope adaptive optics observations of gravitationally lensed quasars in the Sloan Digital Sky Survey*, *ArXiv e-prints* (June, 2015) [arXiv:1506.0514].

[33] E. R. Newton, P. J. Marshall, T. Treu, M. W. Auger, R. Gavazzi, A. S. Bolton, L. V. E. Koopmans, and L. A. Moustakas, *The Sloan Lens ACS Survey. XI. Beyond Hubble Resolution: Size, Luminosity, and Stellar Mass of Compact Lensed Galaxies at Intermediate Redshift*, Astrophys. J. **734** (June, 2011) 104, [arXiv:1104.2608].

[34] M. W. Auger, J. M. Budzynski, V. Belokurov, S. E. Koposov, and I. G. McCarthy, *Are group- and cluster-scale dark matter haloes overconcentrated?*, Mon. Not. R. Astron. Soc. **436** (Nov., 2013) 503–510.

[35] J. Krist, *Tiny Tim : an HST PSF Simulator*, in *Astronomical Data Analysis Software and Systems II* (R. J. Hanisch, R. J. V. Brissenden, and J. Barnes, eds.), vol. 52 of *Astronomical Society of the Pacific Conference Series*, p. 536, Jan., 1993.

[36] P. L. Wizinowich, D. Le Mignant, A. H. Bouchez, R. D. Campbell, J. C. Y. Chin, A. R. Contos, M. A. van Dam, S. K. Hartman, E. M. Johansson, R. E. Lafon, H. Lewis, P. J. Stomski, D. M. Summers, C. G. Brown, P. M. Danforth, C. E. Max, and D. M. Pennington, *The W. M. Keck Observatory Laser Guide Star Adaptive Optics System: Overview*, PASP **118** (Feb., 2006) 297–309.

[37] P. Wizinowich, S. Adkins, R. Dekany, D. Gavel, C. Max, R. Bartos, J. Bell, A. Bouchez, J. Chin, A. Conrad, A. Delacroix, E. Johansson, R. Kupke, C. Lockwood, J. Lyke, F. Marchis, E. McGrath, D. Medeiros, M. Morris, D. Morrison, C. Neyman, S. Panteleev, M. Pollard, M. Reinig, T. Stalcup, S. Thomas, M. Troy, K. Tsubota, V. Velur, K. Wallace, and E. Wetherell, *W. M. Keck Observatory's next-generation adaptive optics facility*, in *Society of Photo-Optical Instrumentation Engineers (SPIE) Conference Series*, vol. 7736 of *Society of Photo-Optical Instrumentation Engineers (SPIE) Conference Series*, p. 0, July, 2010.

[38] J. E. Larkin, A. M. Moore, E. J. Barton, B. Bauman, K. Bui, J. Canfield, D. Crampton, A. Delacroix, M. Fletcher, D. Hale, D. Loop, C. Niehaus, A. C. Phillips, V. Reshetov, L. Simard, R. Smith, R. Suzuki, T. Usuda, and S. A. Wright, *The infrared imaging spectrograph (IRIS) for TMT: instrument overview*, in *Society of Photo-Optical Instrumentation Engineers (SPIE) Conference Series*, vol. 7735 of *Society of Photo-Optical Instrumentation Engineers (SPIE) Conference Series*, p. 29, July, 2010. `arXiv:1007.1973`.

[39] T. Do, S. A. Wright, A. J. Barth, E. J. Barton, L. Simard, J. E. Larkin, A. M. Moore, L. Wang, and B. Ellerbroek, *Prospects for Measuring Supermassive Black Hole Masses with Future Extremely Large Telescopes*, Astron. J. **147** (Apr., 2014) 93, [`arXiv:1401.7988`].

[40] M. Schweitzer, R. Bender, R. Katterloher, F. Eisenhauer, R. Hofmann, R. Saglia, R. Holmes, O. Krause, H.-W. Rix, J. Booth, P. Fagrelius, J. Rhodes, S. Seshadri, A. Refregier, J. Amiaux, J.-L. Augueres, O. Boulade, C. Cara, A. Amara, S. Lilly, E. Atad-Ettedgui, A.-M. di Giorgio, L. Duvet, C. Kuehl, and M. Syed, *NIP: the near infrared imaging photometer for Euclid*, in *Society of Photo-Optical Instrumentation Engineers (SPIE) Conference Series*, vol. 7731 of *Society of Photo-Optical Instrumentation Engineers (SPIE) Conference Series*, p. 1, July, 2010.

[41] M. T. Penny, E. Kerins, N. Rattenbury, J.-P. Beaulieu, A. C. Robin, S. Mao, V. Batista, S. Calchi Novati, A. Cassan, P. Fouqué, I. McDonald, J. B. Marquette, P. Tisserand, and M. R. Zapatero Osorio, *ExELS: an exoplanet legacy science proposal for the ESA Euclid mission - I. Cold exoplanets*, Mon. Not. R. Astron. Soc. **434** (Sept., 2013) 2–22, [`arXiv:1206.5296`].

[42] M. Cropper, S. Pottinger, S.-M. Niemi, J. Denniston, R. Cole, M. Szafraniec, Y. Mellier, M. Berthé, J. Martignac, C. Cara, A. M. di Giorgio, A. Sciortino, S. Paltani, L. Genolet, J.-J. Fourmand, M. Charra, P. Guttridge, B. Winter, J. Endicott, A. Holland, J. Gow, N. Murray, D. Hall, J. Amiaux, R. Laureijs, G. Racca, J.-C. Salvignol, A. Short, J. Lorenzo Alvarez, T. Kitching, H. Hoekstra, and R. Massey, *VIS: the visible imager for Euclid*, in *Society of Photo-Optical Instrumentation Engineers (SPIE) Conference Series*, vol. 9143 of *Society of Photo-Optical Instrumentation Engineers (SPIE) Conference Series*, p. 0, Aug., 2014.

[43] D. Spergel, N. Gehrels, J. Breckinridge, M. Donahue, A. Dressler, B. S. Gaudi, T. Greene, O. Guyon, C. Hirata, J. Kalirai, N. J. Kasdin, W. Moos, S. Perlmutter, M. Postman, B. Rauscher, J. Rhodes, Y. Wang, D. Weinberg, J. Centrella, W. Traub, C. Baltay, J. Colbert, D. Bennett, A. Kiessling, B. Macintosh, J. Merten, M. Mortonson, M. Penny, E. Rozo, D. Savransky, K. Stapelfeldt, Y. Zu, C. Baker, E. Cheng, D. Content, J. Dooley, M. Foote, R. Goullioud, K. Grady, C. Jackson, J. Kruk, M. Levine, M. Melton, C. Peddie, J. Ruffa, and S. Shaklan, *Wide-Field InfraRed Survey Telescope-Astrophysics Focused Telescope Assets WFIRST-AFTA Final Report*, *ArXiv e-prints* (May, 2013) [`arXiv:1305.5422`].

[44] Z. Ivezic, J. A. Tyson, B. Abel, E. Acosta, R. Allsman, Y. AlSayyad, S. F. Anderson, J. Andrew, R. Angel, G. Angeli, R. Ansari, P. Antilogus, K. T. Arndt, P. Astier, E. Aubourg, T. Axelrod, D. J. Bard, J. D. Barr, A. Barrau, J. G. Bartlett, B. J. Bauman, S. Beaumont, A. C. Becker, J. Becla, C. Beldica, S. Bellavia, G. Blanc, R. D. Blandford, J. S. Bloom, J. Bogart, K. Borne, J. F. Bosch, D. Boutigny, W. N. Brandt, M. E. Brown, J. S. Bullock, P. Burchat, D. L. Burke, G. Cagnoli, D. Calabrese, S. Chandrasekharan, S. Chesley, E. C. Cheu, J. Chiang, C. F. Claver, A. J. Connolly, K. H. Cook, A. Cooray, K. R. Covey, C. Cribbs, W. Cui, R. Cutri, G. Daubard, G. Daues, F. Delgado, S. Digel, P. Doherty, R. Dubois, G. P. Dubois-Felsmann, J. Durech, M. Eracleous, H. Ferguson, J. Frank, M. Freemon, E. Gangler, E. Gawiser, J. C. Geary, P. Gee, M. Geha, R. R. Gibson, D. K. Gilmore,

T. Glanzman, I. Goodenow, W. J. Gressler, P. Gris, A. Guyonnet, P. A. Hascall, J. Haupt, F. Hernandez, C. Hogan, D. Huang, M. E. Huffer, W. R. Innes, S. H. Jacoby, B. Jain, J. Jee, J. G. Jernigan, D. Jevremovic, K. Johns, R. L. Jones, C. Juramy-Gilles, M. Juric, S. M. Kahn, J. S. Kalirai, N. Kallivayalil, B. Kalmbach, J. P. Kantor, M. M. Kasliwal, R. Kessler, D. Kirkby, L. Knox, I. Kotov, V. L. Krabbendam, S. Krughoff, P. Kubanek, J. Kuczewski, S. Kulkarni, R. Lambert, L. Le Guillou, D. Levine, M. Liang, K. Lim, C. Lintott, R. H. Lupton, A. Mahabal, P. Marshall, S. Marshall, M. May, R. McKercher, M. Migliore, M. Miller, D. J. Mills, D. G. Monet, M. Moniez, D. R. Neill, J. Nief, A. Nomerotski, M. Nordby, P. O'Connor, J. Oliver, S. S. Olivier, K. Olsen, S. Ortiz, R. E. Owen, R. Pain, J. R. Peterson, C. E. Petry, F. Pierfederici, S. Pietrowicz, R. Pike, P. A. Pinto, R. Plante, S. Plate, P. A. Price, M. Prouza, V. Radeka, J. Rajagopal, A. Rasmussen, N. Regnault, S. T. Ridgway, S. Ritz, W. Rosing, C. Roucelle, M. R. Rumore, S. Russo, A. Saha, B. Sassolas, T. L. Schalk, R. H. Schindler, D. P. Schneider, G. Schumacher, J. Sebag, G. H. Sembroski, L. G. Seppala, I. Shipsey, N. Silvestri, J. A. Smith, R. C. Smith, M. A. Strauss, C. W. Stubbs, D. Sweeney, A. Szalay, P. Takacs, J. J. Thaler, R. Van Berg, D. Vanden Berk, K. Vetter, F. Virieux, B. Xin, L. Walkowicz, C. W. Walter, D. L. Wang, M. Warner, B. Willman, D. Wittman, S. C. Wolff, W. M. Wood-Vasey, P. Yoachim, H. Zhan, and for the LSST Collaboration, *LSST: from Science Drivers to Reference Design and Anticipated Data Products*, *ArXiv e-prints* (May, 2008) [`arXiv:0805.2366`].

[45] A. R. Patnaik, I. W. A. Browne, D. Walsh, F. H. Chaffee, and C. B. Foltz, *B1422+231 - A new gravitationally lensed system at Z = 3.62*, Mon. Not. R. Astron. Soc. **259** (Nov., 1992) 1P–4P.

[46] A. S. Bolton, S. Burles, L. V. E. Koopmans, T. Treu, and L. A. Moustakas, *The Sloan Lens ACS Survey. I. A Large Spectroscopically Selected Sample of Massive Early-Type Lens Galaxies*, Astrophys. J. **638** (Feb., 2006) 703–724, [`astro-ph/0511453`].

[47] T. Treu, L. V. Koopmans, A. S. Bolton, S. Burles, and L. A. Moustakas, *The Sloan Lens ACS Survey. II. Stellar Populations and Internal Structure of Early-Type Lens Galaxies*, Astrophys. J. **640** (Apr., 2006) 662–672, [`astro-ph/0512044`].

[48] L. V. E. Koopmans, T. Treu, A. S. Bolton, S. Burles, and L. A. Moustakas, *The Sloan Lens ACS Survey. III. The Structure and Formation of Early-Type Galaxies and Their Evolution since z ~ 1*, Astrophys. J. **649** (Oct., 2006) 599–615, [`astro-ph/0601628`].

[49] R. Gavazzi, T. Treu, J. D. Rhodes, L. V. E. Koopmans, A. S. Bolton, S. Burles, R. J. Massey, and L. A. Moustakas, *The Sloan Lens ACS Survey. IV. The Mass Density Profile of Early-Type Galaxies out to 100 Effective Radii*, Astrophys. J. **667** (Sept., 2007) 176–190, [`astro-ph/0701589`].

[50] A. S. Bolton, S. Burles, L. V. E. Koopmans, T. Treu, R. Gavazzi, L. A. Moustakas, R. Wayth, and D. J. Schlegel, *The Sloan Lens ACS Survey. V. The Full ACS Strong-Lens Sample*, Astrophys. J. **682** (Aug., 2008) 964–984, [`arXiv:0805.1931`].

[51] R. Gavazzi, T. Treu, L. V. E. Koopmans, A. S. Bolton, L. A. Moustakas, S. Burles, and P. J. Marshall, *The Sloan Lens ACS Survey. VI. Discovery and Analysis of a Double Einstein Ring*, Astrophys. J. **677** (Apr., 2008) 1046–1059, [`arXiv:0801.1555`].

[52] A. S. Bolton, T. Treu, L. V. E. Koopmans, R. Gavazzi, L. A. Moustakas, S. Burles, D. J. Schlegel, and R. Wayth, *The Sloan Lens ACS Survey. VII. Elliptical Galaxy Scaling Laws from Direct Observational Mass Measurements*, Astrophys. J. **684** (Sept., 2008) 248–259, [`arXiv:0805.1932`].

[53] T. Treu, R. Gavazzi, A. Gorecki, P. J. Marshall, L. V. E. Koopmans, A. S. Bolton, L. A. Moustakas, and S. Burles, *The SLACS Survey. VIII. The Relation between Environment and Internal Structure of Early-Type Galaxies*, Astrophys. J. **690** (Jan., 2009) 670–682, [`arXiv:0806.1056`].

[54] M. W. Auger, T. Treu, A. S. Bolton, R. Gavazzi, L. V. E. Koopmans, P. J. Marshall, K. Bundy, and L. A. Moustakas, *The Sloan Lens ACS Survey. IX. Colors, Lensing, and Stellar Masses of Early-Type Galaxies*, Astrophys. J. **705** (Nov., 2009) 1099–1115, [`arXiv:0911.2471`].

[55] M. W. Auger, T. Treu, A. S. Bolton, R. Gavazzi, L. V. E. Koopmans, P. J. Marshall, L. A. Moustakas, and S. Burles, *The Sloan Lens ACS Survey. X. Stellar, Dynamical, and Total Mass Correlations of Massive Early-type Galaxies*, Astrophys. J. **724** (Nov., 2010) 511–525, [`arXiv:1007.2880`].

[56] Y. Shu, A. S. Bolton, J. R. Brownstein, A. D. Montero-Dorta, L. V. E. Koopmans, T. Treu, R. Gavazzi, M. W. Auger, O. Czoske, P. J. Marshall, and L. A. Moustakas, *The Sloan Lens ACS Survey. XII. Extending Strong Lensing to Lower Masses*, ArXiv e-prints (July, 2014) [arXiv:1407.2240].

[57] A. More, R. Cabanac, S. More, C. Alard, M. Limousin, J.-P. Kneib, R. Gavazzi, and V. Motta, *The CFHTLS-Strong Lensing Legacy Survey (SL2S): Investigating the Group-scale Lenses with the SARCS Sample*, Astrophys. J. **749** (Apr., 2012) 38, [arXiv:1109.1821].

[58] R. Gavazzi, T. Treu, P. J. Marshall, F. Brault, and A. Ruff, *The SL2S Galaxy-scale Gravitational Lens Sample. I. The Alignment of Mass and Light in Massive Early-type Galaxies at z = 0.2-0.9*, Astrophys. J. **761** (Dec., 2012) 170, [arXiv:1202.3852].

[59] A. J. Ruff, R. Gavazzi, P. J. Marshall, T. Treu, M. W. Auger, and F. Brault, *The SL2S Galaxy-scale Lens Sample. II. Cosmic Evolution of Dark and Luminous Mass in Early-type Galaxies*, Astrophys. J. **727** (Feb., 2011) 96, [arXiv:1008.3167].

[60] A. Sonnenfeld, R. Gavazzi, S. H. Suyu, T. Treu, and P. J. Marshall, *The SL2S Galaxy-scale Lens Sample. III. Lens Models, Surface Photometry, and Stellar Masses for the Final Sample*, Astrophys. J. **777** (Nov., 2013) 97, [arXiv:1307.4764].

[61] A. Sonnenfeld, T. Treu, R. Gavazzi, S. H. Suyu, P. J. Marshall, M. W. Auger, and C. Nipoti, *The SL2S Galaxy-scale Lens Sample. IV. The Dependence of the Total Mass Density Profile of Early-type Galaxies on Redshift, Stellar Mass, and Size*, Astrophys. J. **777** (Nov., 2013) 98, [arXiv:1307.4759].

[62] A. Sonnenfeld, T. Treu, P. J. Marshall, S. H. Suyu, R. Gavazzi, M. W. Auger, and C. Nipoti, *The SL2S Galaxy-scale Lens Sample. V. Dark Matter Halos and Stellar IMF of Massive Early-type Galaxies Out to Redshift 0.8*, Astrophys. J. **800** (Feb., 2015) 94, [arXiv:1410.1881].

[63] V. N. Bennert, M. W. Auger, T. Treu, J.-H. Woo, and M. A. Malkan, *The Relation between Black Hole Mass and Host Spheroid Stellar Mass Out to z ~ 2*, Astrophys. J. **742** (Dec., 2011) 107, [arXiv:1102.1975].

[64] C. R. Keeton, "GRAVLENS: Computational Methods for Gravitational Lensing." Astrophysics Source Code Library, Feb., 2011.

[65] V. N. Bennert, M. W. Auger, T. Treu, J.-H. Woo, and M. A. Malkan, *A Local Baseline of the Black Hole Mass Scaling Relations for Active Galaxies. I. Methodology and Results of Pilot Study*, Astrophys. J. **726** (Jan., 2011) 59, [arXiv:1008.4602].

[66] J. L. Sérsic, *Influence of the atmospheric and instrumental dispersion on the brightness distribution in a galaxy*, Boletin de la Asociacion Argentina de Astronomia La Plata Argentina **6** (1963) 41.

[67] J. L. Sérsic, *Atlas de galaxias australes*. 1968.

[68] L. Ciotti and G. Bertin, *Analytical properties of the $R^{1/m}$ law*, A&A **352** (Dec., 1999) 447–451, [astro-ph/9911078].

[69] D. Merritt, A. W. Graham, B. Moore, J. Diemand, and B. Terzić, *Empirical Models for Dark Matter Halos. I. Nonparametric Construction of Density Profiles and Comparison with Parametric Models*, Astron. J. **132** (Dec., 2006) 2685–2700, [astro-ph/0509417].

[70] N. W. Evans, *The power-law galaxies*, Mon. Not. R. Astron. Soc. **267** (Mar., 1994) 333–360.

[71] R. Barkana, *Fast Calculation of a Family of Elliptical Mass Gravitational Lens Models*, Astrophys. J. **502** (Aug., 1998) 531–537, [astro-ph/9802002].

[72] T. Schramm, *Realistic elliptical potential wells for gravitational lens models*, A&A **231** (May, 1990) 19–24.

[73] M. W. Auger, T. Treu, B. J. Brewer, and P. J. Marshall, *A compact early-type galaxy at z= 0.6 under a magnifying lens: evidence for inside-out growth*, Mon. Not. R. Astron. Soc. **411** (Feb., 2011) L6–L10, [arXiv:1011.0993].

[74] D. P. Stark, M. Auger, V. Belokurov, T. Jones, B. Robertson, R. S. Ellis, D. J. Sand, A. Moiseev, W. Eagle, and T. Myers, *The CASSOWARY spectroscopy survey: a new sample of gravitationally lensed galaxies in SDSS*, Mon. Not. R. Astron. Soc. **436** (Dec., 2013) 1040–1056, [arXiv:1302.2663].

[75] L. V. E. Koopmans, M. Barnabe, A. Bolton, M. Bradac, L. Ciotti, A. Congdon, O. Czoske, S. Dye, A. Dutton, A. Elliasdottir, E. Evans, C. D. Fassnacht, N. Jackson, C. Keeton, J. Lasio, L. Moustakas, M. Meneghetti, S. Myers, C. Nipoti, S. Suyu, G. van de Ven, S. Vegetti, O. Wucknitz, and H.-S. Zhao, *Strong Gravitational Lensing as a Probe of Gravity, Dark-Matter and Super-Massive Black Holes*, in *astro2010: The Astronomy and Astrophysics Decadal Survey*, vol. 2010 of *Astronomy*, p. 159, 2009. arXiv:0902.3186.

[76] L. Jolissaint, S. Ragland, P. Wizinowich, and A. Bouxin, *Laser guide star adaptive optics point spread function reconstruction project at W. M. Keck Observatory: preliminary on-sky results*, in *Society of Photo-Optical Instrumentation Engineers (SPIE) Conference Series*, vol. 9148 of *Society of Photo-Optical Instrumentation Engineers (SPIE) Conference Series*, p. 4, July, 2014.

[77] G. Herriot, D. Andersen, J. Atwood, C. Boyer, P. Byrnes, K. Caputa, B. Ellerbroek, L. Gilles, A. Hill, Z. Ljusic, J. Pazder, M. Rosensteiner, M. Smith, P. Spano, K. Szeto, J.-P. Véran, I. Wevers, L. Wang, and R. Wooff, *NFIRAOS: first facility AO system for the Thirty Meter Telescope*, in *Society of Photo-Optical Instrumentation Engineers (SPIE) Conference Series*, vol. 9148 of *Society of Photo-Optical Instrumentation Engineers (SPIE) Conference Series*, p. 10, July, 2014. arXiv:1408.4406.

**Table 1**. Telescope and Instrument Properties

| Telescope | Instrument | Filter | Zero Point | Readout Noise (e⁻/pixel) | Background Noise (e⁻/pixel/s) | Pixel Size (arcsec) |
|---|---|---|---|---|---|---|
| HST | ACS | F814W | 25.94 | 4.20 | 0.11 | 0.050 |
| JWST | NIRCAM | F200W | 27.85 | 9.00 | 0.20 | 0.032 |
| LGSAO | NIRC2 | $K'$ | 28.04 | 5.75 | 26 | 0.010 |
| NGAO | NIRC2 | $K'$ | 28.04 | 5.75 | 26 | 0.010 |
| TMT | IRIS | $K'$ | 31.10 | 2.00 | 21 | 0.004 |
| Euclid | VIS | $r+i+z$ | 25.58 | 4.50 | 0.43 | 0.100 |
| WFIRST | — | F184 | 26.18 | 5.00 | 0.11 | 0.110 |
| LSST | — | $I$ | 28.35 | 5.00 | 68 | 0.200 |

Observational facilities (telescopes and instruments) considered in this work. Zero points are given in the ABmag system. The VIS imager of Euclid spans the whole $r + i + z$ wavelength range. The background and exposure time of Euclid will vary across the sky. Our fiducial values are representative of the average performance. The Keck 10-m telescope is considered both with the current (LGSAO) and next-generation (NGAO) adaptive optics capabilities.

**Table 2**. Surface Brightness Profile Models

| Lens Name | $R_{eff}$ (arcsec) | $q$ | P.A. (deg) | $n$ | $\Delta x$ (arcsec) | $\Delta y$ (arcsec) | $m_I$ | $m_K$ | $m_{VIS}$ | $m_H$ |
|---|---|---|---|---|---|---|---|---|---|---|
| Parameters for the source |||||||||||
| fainter system[a] | 0.23 | 0.92 | 54.0 | 4.0 | 0.0662 | -0.167 | 25.0 | 25.0 | 25.0 | 25.0 |
| fainter system[b] | 0.23 | 0.92 | 54.0 | 4.0 | 0.008 | 0.298 | 25.0 | 25.0 | 25.0 | 25.0 |
| brighter system[b] | 0.12 | 0.77 | 120.0 | 1.33 | -0.195 | 0.34 | 22.73 | 22.0 | 23.46 | 22.0 |
| brighter system[a] | 0.12 | 0.77 | 120.0 | 1.33 | 0.01 | -0.005 | 22.73 | 22.0 | 23.46 | 22.0 |
| Parameters for the deflector |||||||||||
| fainter system | 1.76 | 0.61 | -9.6 | 4.0 | — | — | 20.69 | 19.7 | 21.13 | 19.7 |
| brighter system | 0.91 | 0.81 | 113.2 | 4.0 | — | — | 17.99 | 16.5 | 18.84 | 16.5 |

$R_{eff}$ is the half light radius. $q$ denotes the axis ratio. P.A. is with respect to the x-axis. The Sérsic index $n$ controls the degree of curvature of the galaxy light profile. Magnitudes $m$ are given in the ABmag system. The only difference among systems with sources the same brightness is in the source-position, which is set to produce either two or four images of the center.

[a] This configuration yields 4 QSO images.

[b] This configuration yields 2 QSO images.

**Table 3**. Lens Model Parameters

| Lens Name | z | $R_{Ein}$ (arcsec) | q | P.A. (deg) | $\gamma'$ |
|---|---|---|---|---|---|
| fainter system | 0.783 | 1.14 | 0.6 | 14.7 | 2.0 |
| brighter system | 0.351 | 1.1 | 0.81 | 113.2 | 2.0 |

$R_{Ein}$ is the Einstein radius, according to the definition by Kormann+94. $q$ denotes the axis ratio of the mass distribution. P.A. is anti-clockwise from the x-axis. The model deflector is a Singular Isothermal Ellipsoid ($\gamma'$=2), which is then fit using power-law models with variable $\gamma'$.

**Table 4**. Point Source Parameters

|  | mag(I) | mag(K) | mag(VIS) | mag(H) | $\mu$(I) | $\mu$(II) | $\mu$(III) | $\mu$(IV) |
|---|---|---|---|---|---|---|---|---|
| fainter system[a] | 24.0 | 24.0 | 24.0 | 24.0 | 2.84 | 3.75 | 6.59 | 2.78 |
| fainter system[b] | 24.0 | 24.0 | 24.0 | 24.0 | 2.78 | 2.48 | — | — |
| brighter system[b] | 21.7 | 21.5 | 22.9 | 21.5 | 1.22 | 6.10 | — | — |
| brighter system[a] | 21.7 | 21.5 | 22.9 | 21.5 | 6.09 | 8.22 | 6.86 | 7.53 |

Magnitudes (in the ABmag system) and magnifications of multiple images. The source magnitude 'mag' is given in the source plane so that the observed magnitude in the image plane is given by mag $-2.5\log_{10}\mu$, where $\mu$ is the magnification of each image. We just consider TMT observations for the fainter system, and make the point source artificially fainter ($K$=26.0) in order to avoid saturating.

[a] This configuration yields 4 QSO images.
[b] This configuration yields 2 QSO images.

**Table 5**. Exposure time requirements

| Instrument | double | | quad | |
|---|---|---|---|---|
|  | faint | bright | faint | bright |
| HST | $6 \times 10^3$s | 360 s | $3 \times 10^3$s | 150 s |
| JWST | 690s | 180 s | 210s | <60 s |
| Keck (LGSAO) | $105 \times 10^3$s | 3600 s | $75 \times 10^3$s | 2400 s |
| Keck (NGAO) | $18 \times 10^3$s | 180 s | $12 \times 10^3$s | 150 s |
| TMT | 1200s | — | 1080s | — |

Exposure times required to attain a 0.02 precision on the inferred $\gamma'$. The Euclid, WFIRST and LSST surveys, are not quoted here because their exposure times are fixed. The default exposure times are sufficient to meet the 0.02 requirement in the case of LSST and WFIRST, but not for Euclid.

**Table 6**. Precision on the $\gamma'$ with Gaussian and Moffat PSF for WFIRST

| Lens Name | Gaussian | Moffat ($\beta$=1.5) | Moffat ($\beta$=3.0) | Moffat ($\beta$=4.5) | Moffat ($\beta$=6.0) |
|---|---|---|---|---|---|
| fainter system[a] | 0.021 | 0.032 | 0.028 | 0.025 | 0.023 |
| fainter system[b] | 0.023 | 0.036 | 0.035 | 0.033 | 0.030 |
| brighter system[b] | 0.0044 | 0.0065 | 0.0062 | 0.0048 | 0.0044 |
| brighter system[a] | 0.0016 | 0.0022 | 0.0017 | 0.0017 | 0.0015 |

Precision on the mass density profile slope $\gamma'$ with Gaussian and Moffat PSFs for WFIRST. This table represents the results for fainter and brighter systems with 4 and 2 QSO images. It is shown that as $\beta$ increases the Moffat PSF tends to approximate the core of the Gaussian PSF.

[a] This configuration yields 4 QSO images.
[b] This configuration yields 2 QSO images.
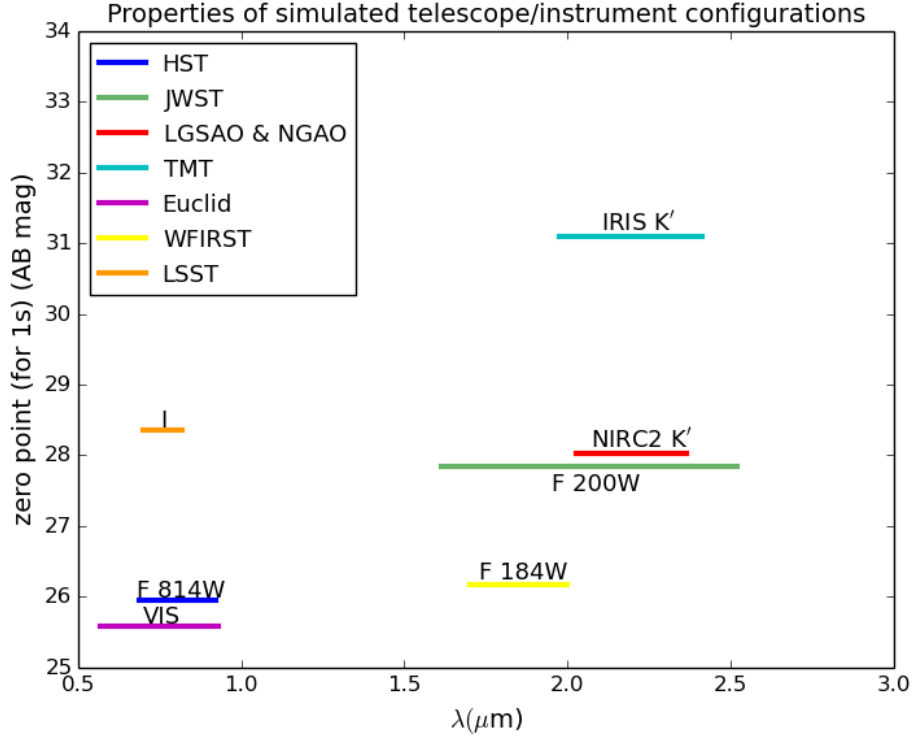
**Figure 1**. Zero points in AB magnitudes for HST/ACS (blue), JWST/NIRCAM (green), Keck NIRC2 (assumed for both LGSAO and NGAO; red), TMT/IRIS (cyan), Euclid (magenta), WFIRST (yellow) and LSST (orange), corresponding to one count per second. The colored bars indicate the wavelength range of each instrumental setup considered in this work.
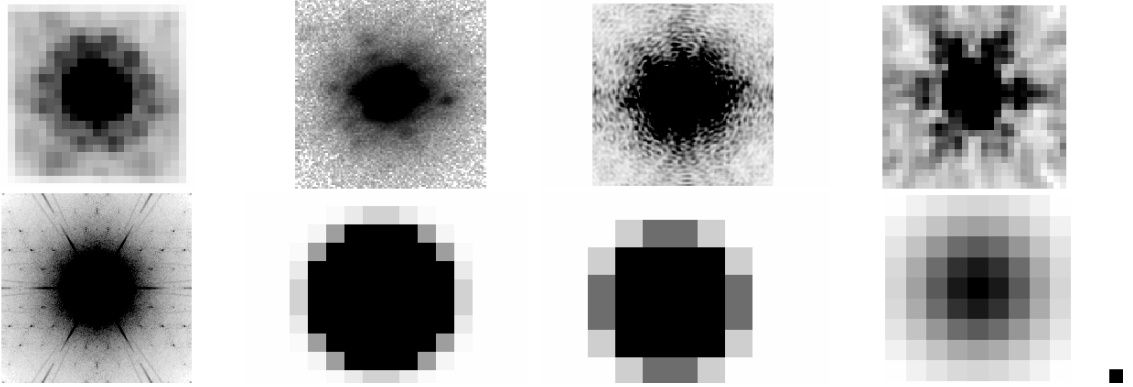


**Figure 2**. Montage of the point spread functions (PSFs) of each instrument. The upper row, from left to right, represents HST/ACS, Keck/NIRC2+LGSAO, Keck/NIRC2+NGAO, and JWST/NIRCAM. The lower row, from left to right, shows TMT/IRIS, Euclid, WFIRST, and LSST, respectively. Observed or simulated PSFs are used for HST, JWST, Keck (LGSAO & NGAO), and TMT. Gaussian PSFs are adopted for the other three survey instruments.
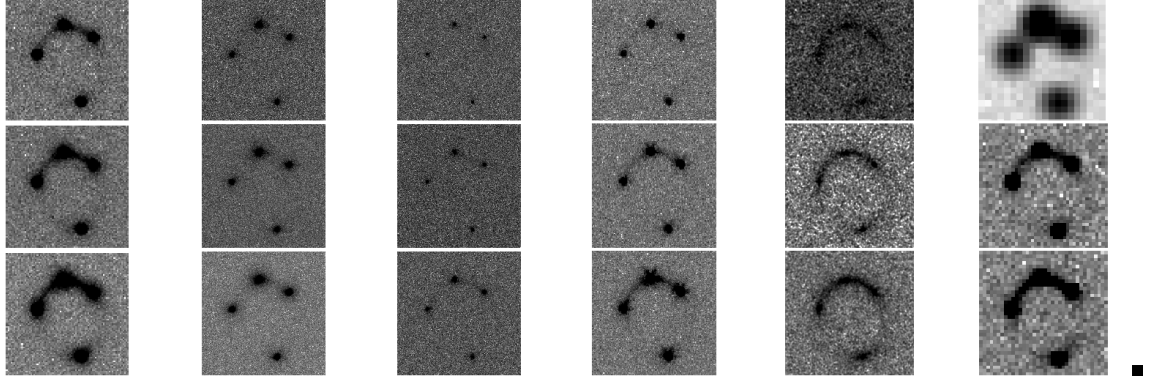
**Figure 3**. Simulations of the fainter lens system with 4 QSO images. The simulated images are all 4″ × 4″. The first 5 columns, from left to right, represent HST/ACS, Keck/NIRC2+LGSAO, Keck/NIRC2+NGAO, JWST/NIRCAM, and TMT; from top to bottom, the rows correspond to 1/3 × "target" exposure time, "target" exposure time, and 3 × "target" exposure time. "Target" exposure time is defined as the exposure time that yields 2% precision on the slope of the mass density profile of the mass model $\gamma'$. The sixth column shows simulations of 3 surveys. From top to bottom we show LSST, Euclid, and WFIRST, with the default survey exposure times (4500s, 2360s, 920s, respectively).
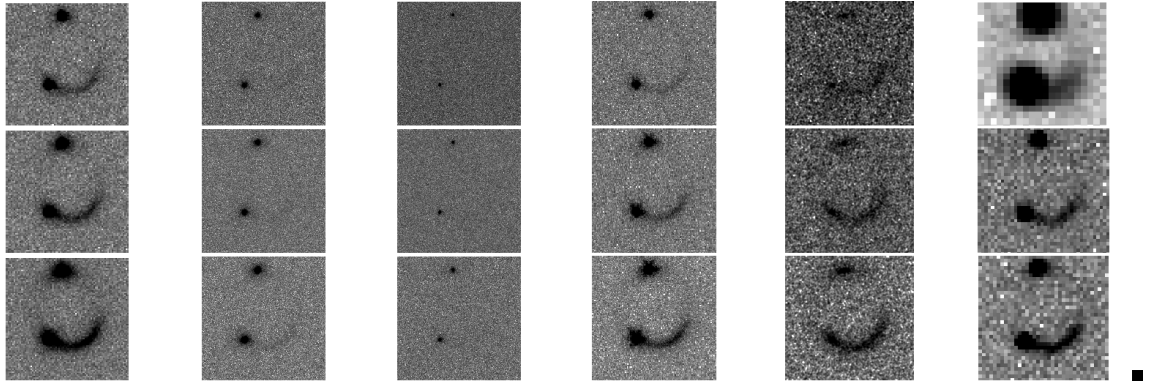


**Figure 4**. Same as Fig. 3, for the faint double system.
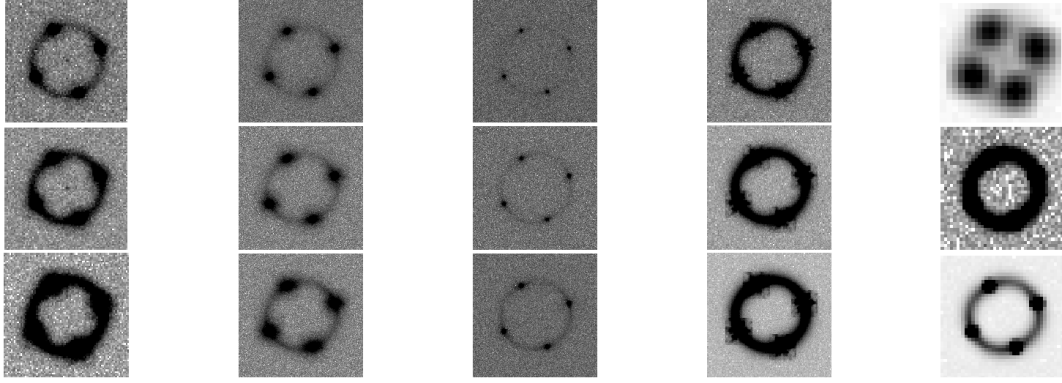
**Figure 5.** Simulations of the bright lens system with 4 QSO images. The simulated images are all 4″ × 4″. The first 3 columns, from left to right, represent HST/ACS, Keck/NIRC2+LGSAO, Keck/NIRC2+NGAO; from top to bottom, the rows correspond to 1/3 × "target" exposure time, "target" exposure time, and 3 × "target" exposure time. "Target" exposure time is defined as the exposure time that yields 2% precision on the slope of the mass density profile of the mass model $\gamma'$. The fourth column shows JWST simulations with 3 fixed exposure times: 60, 180, 540 seconds, from top to bottom. The fifth column shows simulations of 3 surveys. From top to bottom we show LSST, Euclid, and WFIRST, with the default survey exposure times (4500s, 2360s, 920s, respectively). TMT simulations are not shown since the system is considered too bright to be observed with this telescope in practice.
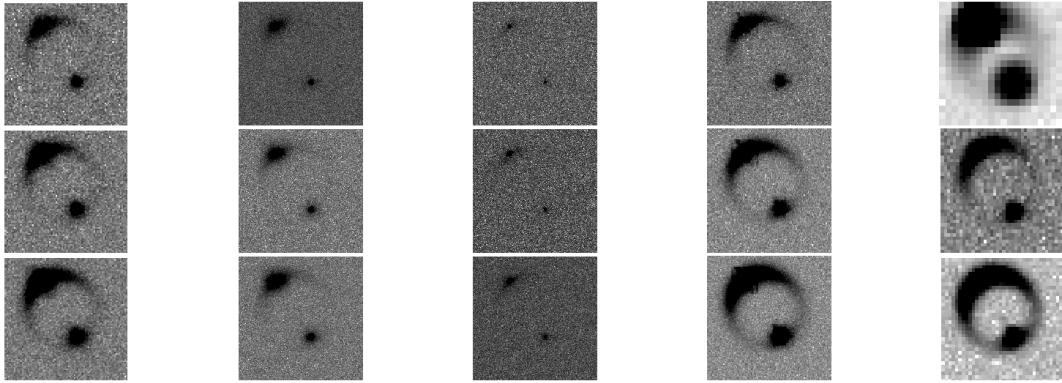


**Figure 6.** Same as Fig. 5, for the bright double imaged system.
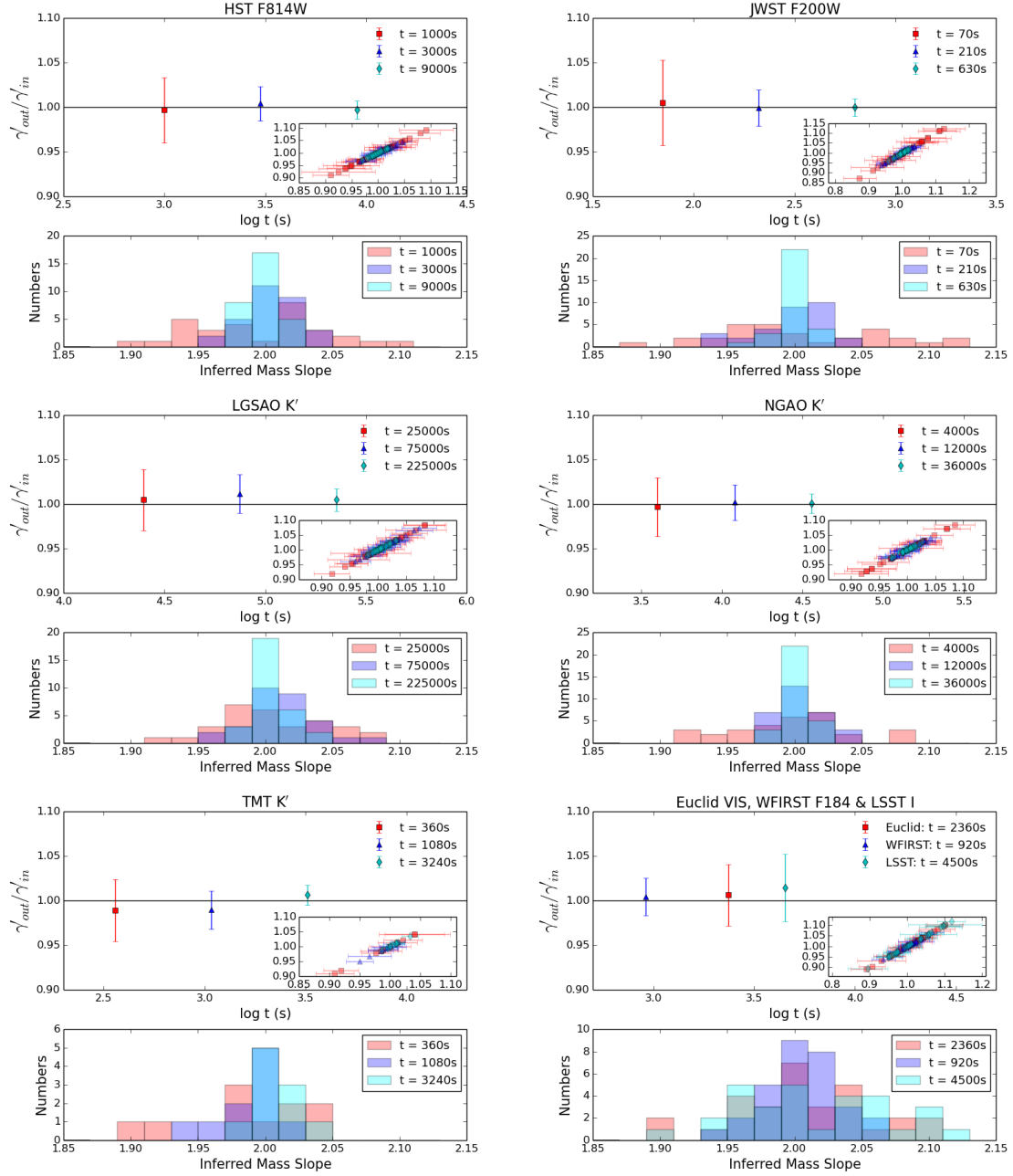
**Figure 7**. Precision on the mass density profile slope $\gamma'$ as a function of exposure time. This figure shows the results for the fainter lens system with 4 QSO images. The quantity $\gamma'_{in}$ is the input SIE mass slope. The quantity $\gamma'_{out}$ is the output of the inference process. The insert in each panel shows all 30 simulation results (10 simulation results for TMT) for each exposure time with the same color coding. Note that both axes represent $\gamma'_{out}/\gamma'_{in}$ whereas error bars are only shown on the x-axis for clarity. The histogram in each panel represents the distribution of inferred mass slope more directly.
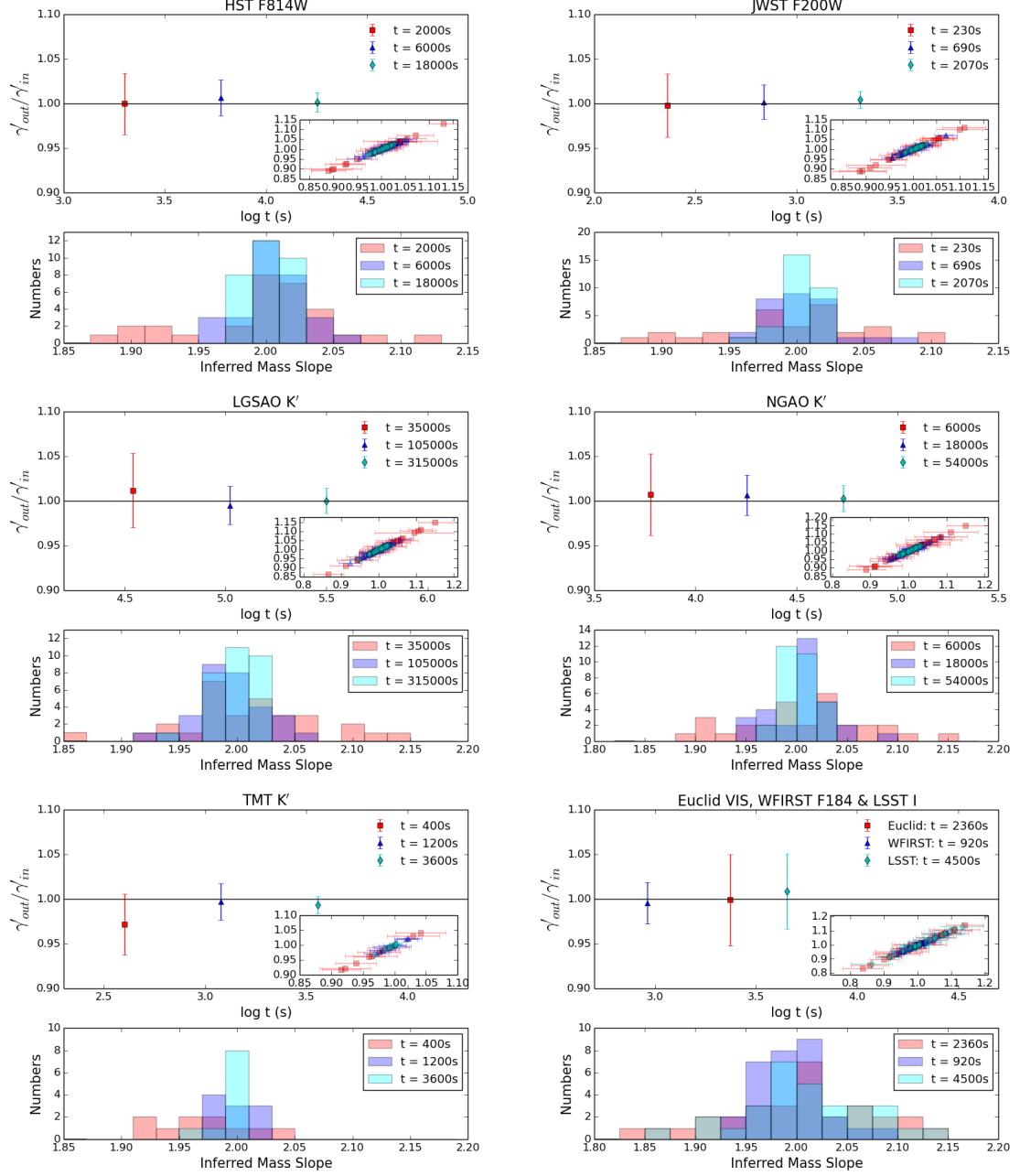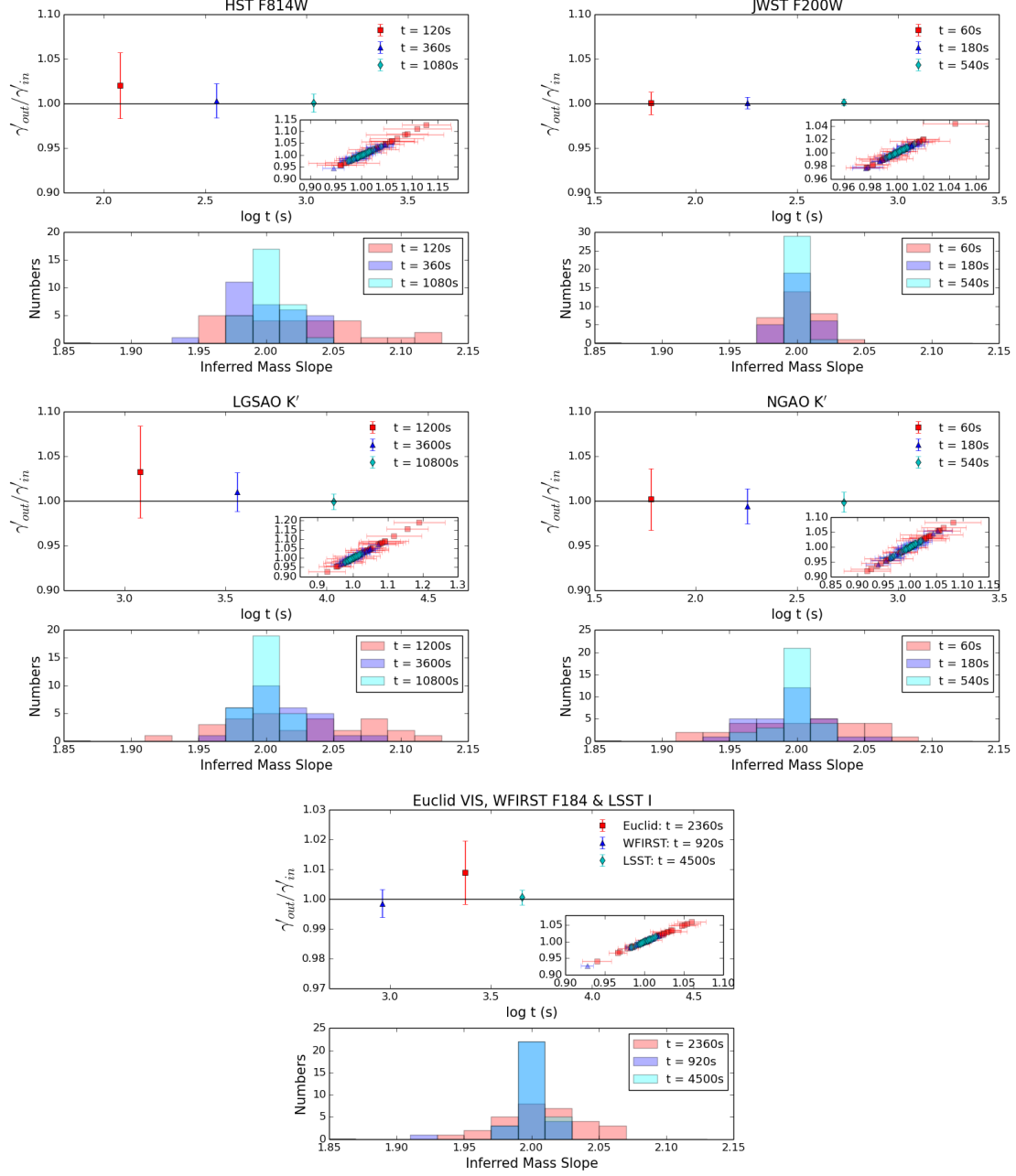
**Figure 8**. Same as Fig. 7 for the fainter lens system with 2 images.
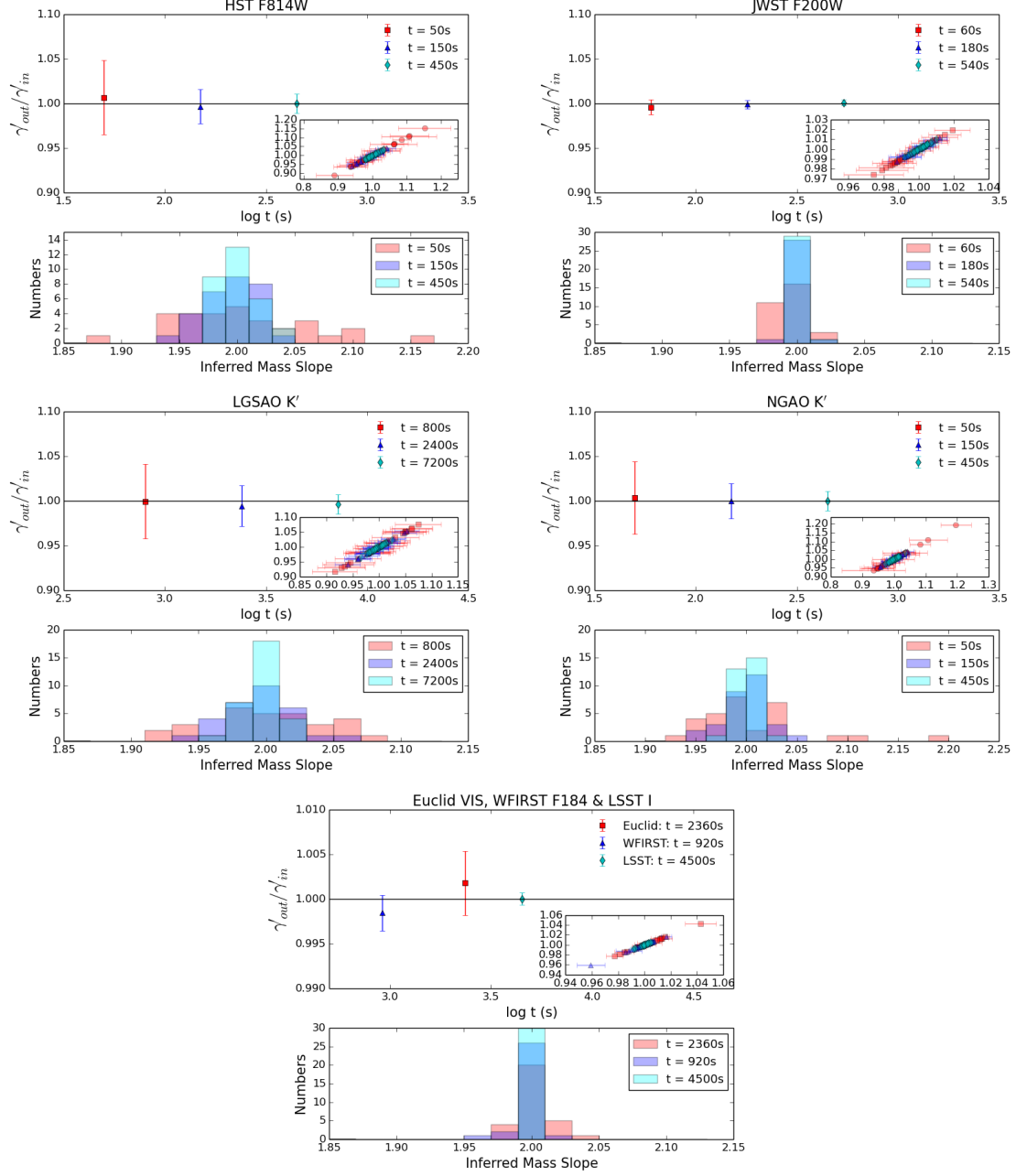
**Figure 9**. Same as Fig. 7 for the brighter lens system with 4 images.

**Figure 10**. Same as Fig. 7 for the brighter lens system with 2 images.